Cellular/Molecular

A Role for Presenilins in Autophagy Revisited: Normal Acidification of Lysosomes in Cells Lacking *PSEN1* and *PSEN2*

Xulun Zhang,[1] Krassimira Garbett,[2] Karthikeyan Veeraraghavalu,[1] Brian Wilburn,[1] Reid Gilmore,[3] Karoly Mirnics,[2] and Sangram S. Sisodia[1]

[1]Department of Neurobiology, The University of Chicago, Chicago, Illinois 60637, [2]Department of Psychiatry, Vanderbilt University, Nashville, Tennessee 37232, and [3]Department of Biochemistry and Molecular Pharmacology, University of Massachusetts Medical School, Worcester, Massachusetts 01605

Presenilins 1 and 2 (PS1 and PS2) are the catalytic subunits of the γ-secretase complex, and genes encoding mutant PS1 and PS2 variants cause familial forms of Alzheimer's disease. Lee et al. (2010) recently reported that loss of PS1 activity lead to impairments in autophagosomal function as a consequence of lysosomal alkalinization, caused by failed maturation of the proton translocating V0a1 subunit of the vacuolar (H+)-ATPase and targeting to the lysosome. We have reexamined these issues in mammalian cells and in brains of mice lacking PS (PScdko) and have been unable to find evidence that the turnover of autophagic substrates, vesicle pH, V0a1 maturation, or lysosome function is altered compared with wild-type counterparts. Collectively, our studies fail to document a role for presenilins in regulating cellular autophagosomal function. On the other hand, our transcriptome studies of PScdko mouse brains reveal, for the first time, a role for PS in regulating lysosomal biogenesis.

Introduction

Presenilins are polytopic membrane proteins that serve as the catalytic center of γ-secretase (Ahn et al., 2010), an enzyme complex that catalyzes intramembranous proteolysis of a variety of type I membrane substrates (for review, see De Strooper, 2003). Importantly, inheritance of mutations in the *PSEN1* gene and the homolog, *PSEN2*, causes early onset, autosomal dominant, familial forms of Alzheimer's disease (FAD).

In addition to a role as the catalytic subunit of "γ-secretase," studies have shown that PS plays a role in several diverse cellular processes, including autophagy (for review, see De Strooper and Annaert, 2010). In this regard, Lee et al. (2010) reported that in *PSEN1*-null (PS1ko) blastocysts, and brains of mice with reduced levels of PS1, the degradation of long-lived proteins was impaired, while the clearance of autophagosomes during macroautophagy was prevented. Lee et al. (2010) reported that these defects were the consequence of impaired lysosomal acidification resulting from failed oligosaccharide maturation and subsequent transport of the proton translocating V0a1 subunit of the vacuolar (H+)-ATPase (v-ATPase) to the lysosome. At a mechanistic level, the authors reported that full-length PS1 bound to V0a1 subunit in the ER, thus facilitating N-glycosylation by the STT3B subunit of the oligosaccharyltransferase (OST) complex. Finally, Lee et al. (2010) reported that expression of FAD-linked PS1 variants in patient fibroblasts exhibited impairments in macroautophagy and targeting of V0a1 to lysosomes.

In view of the substantial implications of these latter findings for understanding the functions of presenilins in health and AD, we sought to reexamine these issues. In contrast to the findings reported by Lee et al. (2010), we now document that the turnover of established autophagic substrates is apparently unperturbed in embryonic stem (ES) cells lacking *PSEN1* (PS1ko-ES) or both *PSEN1* and *PSEN2* (PSdko-ES) compared with WT-ES cells. In addition, we demonstrate that mean vesicle pH in cultured PS1ko-ES cells and PSdko-ES cells is very similar to that in cultured WT-ES cells. Indeed, V0a1 maturation and acidic pH-dependent, lysosomal maturation of CatD is indistinguishable between cultured WT-ES, PS1ko-ES, and PSdko-ES cells, and in the hippocampi of mice with genetic deletions of *PSEN1* and *PSEN2* in excitatory neurons (PScdko mice) compared with their littermate controls. Similarly, V0a1 maturation and CatD processing are unimpaired in stable cell lines or brains of transgenic mice expressing PS1 variants. Finally, we neither confirm an association of PS1 holoprotein with either V0a1 and/or STT3B, nor that V0a1 is uniquely glycosylated by STT3B. Collectively, our studies fail to document a role for presenilins in regulating cellular autophagosomal function.

Last, we document that the expression of transcripts encoding TFEB, a master transcriptional regulator of lysosomal biogenesis and autophagy, is no different between cultured PSdko-ES and WT-ES cells, or in brains of PScdko mice compared with littermate controls. However, the expression of a set of genes within

Received Feb. 5, 2012; revised April 26, 2012; accepted April 30, 2012.

Author contributions: X.Z. and S.S.S. designed research; X.Z., K.G., K.V., and B.W. performed research; X.Z., K.G., K.V., B.W., R.G., K.M., and S.S.S. analyzed data; S.S.S. wrote the paper.

These studies were supported by NIH Grant R01-AG021494 (S.S.S. and K.M.), the Adler Foundation (K.V.), Edward H. Levi Fund (K.V. and X.Z.), and Cure Alzheimer's Fund (S.S.S.).

S.S.S. discloses that he is a paid consultant of Nociris Inc. and Eisai Research Labs Inc., but does not hold shares in any company that is a maker or owner of a FDA-regulated drug or device.

Correspondence should be addressed to Sangram S. Sisodia at the above address. E-mail: ssisodia@bsd.uchicago.edu.

DOI:10.1523/JNEUROSCI.0556-12.2012

 0270-6474/12/328633-16$15.00/0

the Coordinated Lysosomal Expression and Regulation (CLEAR) network is significantly upregulated in the brains of mice lacking *PSEN* expression in excitatory neurons, findings that would argue that PS plays a critical role in regulating lysosomal biogenesis, but in a TFEB mRNA expression-independent manner.

Materials and Methods

Cell lines, plasmids, and transfection. HEK293 cells, wild-type, PS1ko, and PSdko mouse embryo fibroblasts (MEFs) were cultured in DMEM (Invitrogen) containing 10% FBS (Invitrogen) and 1× penicillin/streptomycin (Invitrogen). PEN-2 knockdown cells were obtained from Dr. Harald Steiner (Ludwig Maximilians Universität München, Munich, Germany) (Prokop et al., 2004). Early passage WT-ES, PS1ko-ES, and PSdko-ES cells were obtained from Dr. Bruce Yankner (Harvard Medical School, Boston, MA) (Zhang et al., 2000) and were cultured in DMEM containing 15% FBS, 1× nonessential amino acids (Invitrogen), 2 mM glutamine (Invitrogen), 1× penicillin/streptomycin, 1 mM sodium pyruvate (Invitrogen), 1000units/ml LIF (Millipore), and 100 μM β-mercaptoethanol (Sigma). N2a cells were cultured in 50% DMEM and 50% Optimem (Invitrogen) containing 10% FBS and penicillin/streptomycin. The brain-specific human V0a1 cDNA was obtained from the functional genomics facility at the University of Chicago and cloned into expression vector pAG3 with a myc-6xHis tag at its C terminus. WT and PSdko MEFs were stably transfected with human V0a1-myc-6xHis plasmid using Lipofectamine and plus reagent (Invitrogen), and the selected positive pool was then cultured in DMEM containing 10% FBS, penicillin/streptomycin, and 200 μg/ml zeocin (Invitrogen). Human V0a1-myc-6xHis plasmid was transiently transfected into cultured WT-ES, PS1ko-ES, and PSdko-ES cells using Lipofectamine 2000 (Invitrogen), and cells were harvested 48 h after transfection for Western blot analysis. To determine transient transfection efficiencies, a plasmid encoding GFP was transfected as a control.

Experimental animals. The generation of forebrain-specific *PSEN* conditional double knock-out mice (PScdko mice) has been described previously (Mirnics et al., 2008), and 6-month-old male animals were used for microarray and Western blot analysis. Transgenic mice expressing mouse prion (PrP) promoter-driven human wild-type PS1, human PS1ΔE9, and human PS1M146L were described previously (Thinakaran et al., 1996; Lee et al., 1997; Choi et al., 2008), and male animals were used for Western blot analysis. Homozygous *Gt[ROSA]26Sor*$^{tm4[ACTB-tdTomato,-EGFP]Luo}$ mice (Muzumdar et al., 2007) were crossed to *calmodulin kinase II gene promoter* (*CaMKII-cre*) transgenic mouse line and 5-week-old bigenic male offspring were examined for *cre*-induced recombination. All experimental procedures were reviewed and approved by Institutional Animal Care and Use Committee (IACUC) of the University of Chicago (Protocol #s 71434 and 70958).

Quantitative PCR analysis. Total RNA was isolated from MEF and ES cells using Trizol reagent (Invitrogen), and the isolated RNA was treated with RQ1 RNase-free DNase to remove residual DNA. First-strand cDNA was synthesized with SuperScript III first-strand synthesis system (Invitrogen) following the manufacturer's instructions. The primers used for TFEB quantitative PCR (qPCR) are as follows: mouse TFEB forward (Fw): AAGCAGCTCTGGCTCCGCAT, mouse TFEB reverse (Rv): CGGCATTTGCTCAGGCTCAG. The primers used for CatD qPCR are as follows: mouse CatD Fw: AAGGGCAACCCGGAGGAGAA, mouse CatD Rv: TTCCACAGGCCCCACCAG AA. QPCRs of TFEB and CatD transcripts in MEF and/or ES cells were performed with RT^2 SYBR Green Fluor qPCR Mastermix (Qiagen, 330510) on an iCycler iQ Real-Time PCR detection system (Bio-Rad). GAPDH was used as an internal control. $\Delta\Delta C_T$ method was used to compare the transcript level of TFEB in WT and PSdko cells.

RNA isolation and gene expression analyses. ES Cell transcriptome analysis: RNA from ES cells was processed with Single-Round RNA Amplification and Biotin Labeling System (Enzo Life Sciences) and then hybridized on a GeneChip HT MG-430 P.M. 24-Array Plate (Affymetrix), using two replicates for each condition. Agilent Bioanalyzer assessment reported RNA integrity numbers (RIN) of 9 or above. The data were log2 transformed using RMA. Average log2 ratios (ALRs) were calculated for each gene using the replicates. The distribution of ALRs from the autophagy and CLEAR gene groups was compared with the overall distribution of all ALRs obtained in the experiment using a groupwise, two-tailed *t* test. PScdko mice transcriptome analysis: This dataset is described in detail in the study by Mirnics et al. (2008). We used previously profiled samples from the hippocampi and frontal cortices of 6-month-old PScdko and control animals. Distribution of the ALRs from the autophagy and CLEAR gene groups was assessed using the same method as described above for the ES cells.

siRNAs and antibodies. STT3A and STT3B siRNAs and anti-STT3A or -STT3B antibodies were described previously (Ruiz-Canada et al., 2009). Anti-PSAP antibody was obtained from Dr. Shahriar Koochekpour (Roswell Park Cancer Institute, Buffalo, NY) (Hu et al., 2010). Anti-Cathepsin C (D-6, s.c.-74590), anti-Cathepsin D (C-20, s.c.-6486), anti-OST48 (E-9, s.c.-74408), and anti-actin (SPM161, s.c.-56459) antibodies were purchased from Santa Cruz Biotechnology. Anti-V0a1 polyclonal antibody was purchased from Synaptic Systems. Anti-6XHis tag polyclonal antibody was purchased from Rockland Immunochemicals. Anti-LC3 antibody (PM036) was purchased from MBL International. P62 antibody (P0067) was purchased from Sigma. Polyclonal anti-PS1 NT antibody recognizes amino acids 1–65 (Kim and Sisodia, 2005), and rat anti-human PS1 antibody was a kind gift from Dr. Allan Levey (Emory University, Atlanta, GA). APP antibody 369 was a kind gift from Dr. Sam Gandy (Mount Sinai School of Medicine, New York, NY).

Western blotting. Cells and brain samples were lysed or homogenized in lysis buffer containing 50 mM Tris-HCl pH7.4, 150 mM NaCl, 0.5% NP40, 0.5% sodium deoxycholate, 5 mM EDTA, and protease inhibitor cocktail (Sigma). Protein concentrations were determined by BCA kit (Pierce). Equal amount of protein lysates were resolve by SDS-PAGE and transferred to a nitrocellulose membrane. After blocking, the membrane was sequentially incubated with primary and secondary antibodies, and bound antibodies were detected by electrochemiluminescence (ECL; PerkinElmer).

STT3A and STT3B knockdown in HEK293 cells. HEK293 cells were repeatedly transfected with 30 nM STT3A or STT3B siRNAs with RNAiMax (Invitrogen). Human V0a1-myc-6xHis was also transfected into these cells with Lipofectamine 2000 after the initial siRNA transfection to analyze the glycosylation of V0a1 in the presence or absence of STT3A or STT3B.

PNGase F and Endo H treatment. For PNGase F treatment, cell lysates were first supplemented with glycoprotein denaturation buffer (0.5% SDS, 40 mM DTT) and incubated at room temperature for 10 min. NP40 was then added to the mixture to a final concentration of 1%. G7 buffer (50 mM Sodium Phosphate, pH 7.5) and PNGase F (100 U) (New England Biolabs) were then added to the mixture and incubated for 1 h at 37°C. For Endo H treatment, cell lysates were supplemented with glycoprotein denaturation buffer and incubated at room temperature for 10 min; G5 buffer (50 mM Sodium Citrate, pH 5.5) and Endo H (200 U) (New England Biolabs) were then added to the mixture and incubated for 1 h at 37°C. The PNGase F and Endo H reactions were quenched by the addition of 4× Laemmli sample buffer.

Pulse labeling. Following transfection with siRNA and cDNA encoding human V0a1–6His, HEK293 cells were labeled for 30 min with 250 μCi ^{35}S-methionine (PerkinElmer). Cells were lysed in lysis buffer (Tris-HCl pH7.4, 150 mM NaCl, 5 mM EDTA, 0.5% NP40, and 0.5% sodium deoxycholate and protease inhibitor cocktail) and the total radioactivity (cpm) was determined after TCA precipitation and liquid scintillation counting. Equal cpm of cell lysates was used for V0a1 immunoprecipitation. Immunoprecipitated proteins were resolved on 6% SDS-PAGE, transferred to a nitrocellulose membrane, and exposed to a PhosphorImager screen. The screen was scanned using a Storm Imager (GE Healthcare). Imagequant 5.0 software was used for the image analysis.

Autophagy studies. Mouse ES cells were seeded so that they reached ~90% confluence at the time of lysis and protein extraction. To induce autophagy, ES cells were starved by incubation in ES medium without FBS for 6 h. To examine autophagic flux, ES cells were treated with bafilomycin A1 (Sigma) at 100 nM for the last 3 h of starvation. LC3 and p62 band intensities were quantified and normalized to actin using ImageJ software.

Fluorescent microscopy and image processing. ES cells were seeded in glass bottom culture dishes (Mat Tek) so they would be ~50–70% confluent at the time of imaging (~18 h). Cells were incubated in 1 μM Lysosensor Yellow/Blue DND-160 (Invitrogen) for 5 min. Cells were then washed twice in PBS followed by twice in clamp buffer (5 mM NaCl, 115 mM KCl, 1.2 mM $MgSO_4$, 25 mM MES, pH 3.5–7.5). Cells were equilibrated in clamp buffer pH7.5 supplemented with 25 μM monensin (Sigma) for 20 min before imaging. The same dish of cells was then washed twice with clamp buffer (pH6.0) and then allowed to equilibrate for 10 min before imaging. This process was repeated for all clamp buffers (pH7.5–3.5). All equilibration steps were performed in a 37°C, 5% CO_2 incubator. Imaging was performed on a heated stage (37°C). Cells were excited with attenuated UV light (357–373 nm) and observed in blue (W1; 417–483 nm) and yellow (W2; 490–530 nm) region of the spectra. Five 60× images were collected over a period of 5 min for each pH. Sixteen-bit images were processed to subtract background fluorescence, and then ratio (W1/W2) images were generated using the image calculator function in ImageJ. Regions of interest (ROIs) corresponding to vesicles were generated using W2 and applied to ratio images to determine the W1/W2 ratio value of the vesicles for each pH clamp buffer. A standard curve was generated in Prism to assign a predicted pH for relevant W1/W2 values. An independent standard curve was generated on each experimental day. For test groups, cells were incubated in 1 μM Lysosensor Yellow/Blue DND-160 for 5 min, washed twice in PBS, and 15 60× images were collected and analyzed, as above.

Immunofluorescence staining of brain sections. Brain coronal sections (45 μm) were cut on a prechilled sliding microtome block (Leica), and the floating sections were immunostained with either anti-NeuN monoclonal antibody (1:800; Millipore) or anti-βIII Tubulin TUJ1 monoclonal antibody (1:500; Covance) as described previously (Choi et al., 2008). Stained sections were visualized using DyLight-549 conjugated donkey anti-mouse antibody (1:400; Jackson ImmunoResearch) and were counter stained with DAPI (1:15000; 4′, 6-diamidine-2′-phenylindole dihydrochloride, Roche Biochemicals). Both mTomato red or mEGFP expressing cells were bright enough for direct microscopic analysis.

Statistical analysis. Data are expressed as mean values ± SEM.

Results

Autophagy substrates are degraded efficiently in blastocyst-derived ES cell cultures that lack *PSEN1* or both *PSEN1* and *PSEN2*

Microtubule-associated protein 1 (LC3) is widely used as a marker for autophagosomes and migrates as an ~16 kDa "unprocessed" form, termed LC3-I, and an ~16 phosphatidylethanolamine-derivatized LC3-II species by SDS-PAGE. The amount of LC3-II usually correlates well with the number of autophagosomes, or more precisely, the level of LC3-II bound to autophagic membranes (Kabeya et al., 2000). Lee et al. (2010) revealed that in nutrient-rich conditions, PS1ko blastocysts exhibited a twofold increase in the levels of LC3-II compared with the LC3-II levels in wild-type (WT) blastocysts. Moreover, induction of autophagy by serum withdrawal resulted in higher LC3-II levels in WT cells, but to a much lesser extent in PS1 KO cells. Finally, to assess autophagic "flux," Lee et al. (2010) treated WT and PS1ko blastocysts with leupeptin to inhibit cysteine proteases in autophagolysosomes; LC3-II is degraded in autophagolysosomes and hence, LC3II turnover is thought to be a reliable measure of autophagic activity (Mizushima et al., 2010). In this case, Lee et al. (2010) showed that while leupeptin-treated WT cells showed a clear elevation of LC3II, the levels of LC3-II in PS1ko cells were unchanged over baseline. Finally, the authors examined the levels of p62/A170/SQSTM1 (hereafter termed p62) that binds to ubiquitinated proteins in the cytosol and directly interacts with LC3 that is bound to the isolation membrane/phagaphore; this LC3-p62 complex is subsequently degraded by autophagolysosomes (Ichimura et al., 2008). In this setting, Lee et al. (2010) reported that p62 levels were elevated in PS1ko cells compared with those in WT cells, suggestive of a defect in autophagic clearance. Together, the authors concluded that PS1ko cells had a deficit in the clearance of autophagosomal vacuoles containing LC3-II and p62.

We were intrigued by the results obtained by Lee et al. (2010) because PS1ko cells constitutively express the functionally homologous PS2 protein, and hence, we surmised that the reported effects on LC3-II and p62 levels might have been underestimated. To activate autophagy, we serum-starved cultured PS1ko-ES, cultured ES cells wherein *PSEN1* and *PSEN2* are disrupted (PSdko-ES cells), and cultured WT-ES cells for 6 h and assessed the levels of the autophagy substrates LC3-II and p62. In addition, we examined LC3-II or p62 levels in serum-starved cells either in the absence, or presence of bafilomycin A1, an agent that inhibits lysosomal acidification and/or inhibits autophagosome-lysosome fusion; this treatment leads to reduced degradation and hence, accumulation of autophagy substrates (Tanida et al., 2005).

Much to our surprise, and in striking contrast to the results obtained by Lee et al. (2010), upon serum starvation, we observed a significant reduction in LC3-II levels in cultured PS1ko-ES cells compared with cultured WT-ES cells, and this level was reduced further in cultured PSdko-ES cells (Fig. 1*A*, compare lanes 1, 3 and 5, respectively). Our demonstration of lower LC3-II levels in cultured PS1ko-ES and PSdko-ES cells could be interpreted to suggest that autophagosome membranes are limiting, or that LC3-II is rapidly degraded in autophagolysosomes following fusion of autophagosomes with lysosomes. To address this issue, we assessed "autophagic flux," a measure of autophagic activity (Mizushima et al., 2010). To examine autophagic flux, we treated serum-starved cells with bafilomycin; the differences in the amount of LC3-II between samples in the presence and absence of bafilomycin A1 represent the amount of LC3 that is delivered to lysosomes for degradation (Klionsky et al., 2008; Mizushima and Yoshimori, 2007; Rubinsztein et al., 2009). In this case, we observed that LC3-II levels were elevated in cultured WT-ES cells (Fig. 1*A*, compare lanes 1, 2) as expected, but even more remarkably, the levels of LC3-II were substantially elevated in the cultured PS1ko-ES and PS1dko-ES cells compared with the levels observed in respective cells maintained in starvation conditions (Fig. 1*A*, compare lanes 3, 4 and 5, 6, respectively; quantified in *B*, *C*). Hence, these studies reveal that the reduced steady-state level of LC3-II in serum-starved cultured PS1ko-ES and PSdko-ES cells is the result of elevated autophagolysosomal activity in these cells compared with cultured WT-ES cells, thus arguing that autophagosomal activity in cultured PS1ko-ES and PSdko-ES cells is unimpaired.

To validate these latter conclusions, we examined the turnover of p62, in serum-starved cultured WT-ES, PS1ko-ES, and PSdko-ES cells either in the absence, or presence of bafilomycin. Under these conditions, we observed that compared with serum-starved cultured WT-ES cells, the steady-state levels of p62 were slightly elevated in serum-starved cultured PS1ko-ES and PSdko-ES cells (Fig. 1*D*, compare lanes 1, 3, 5, respectively), as was previously reported (Lee et al., 2010). While the elevation in levels of p62 in the cultured PS1ko-ES and PSdko-ES cells may be indicative of autophagy failure, as was claimed earlier (Lee et al., 2010), it was necessary to confirm this proposal using the autophagic flux assay. In this regard, treatment of starved cells with bafilomycin revealed a clear elevation in p62 levels in all cell lines analyzed (Fig. 1*D*, compare lanes 1 and 2, 3 and 4, 5 and 6 respectively; quantified in *E*, *F*). We confirmed the lack of expression of

PS1 in the PS1ko-ES and PSdko-ES cells by Western blot analyses (Fig. 1*G*, lanes 3–6). In parallel, and due to very low levels of PS2 detected with our antibodies in ES cell lysates, we chose to employ RT-PCR to confirm the lack of *PSEN2* mRNA in PSdko-ES cells (Fig. 1*H*, lane 4; compare to lanes 2, 3).

Collectively, our autophagic flux analyses of p62 and LC3-II lead us to conclude that autophagy is as active in the cultured PS1ko-ES and PSdko-ES cells.

Mean vesicle pH in cultured WT-ES and PS1ko-ES Cells are equivalent, but is slightly more acidic in cultured PSdko-ES cells

In an attempt to demonstrate that the defects in autophagy seen in PS1ko blastocysts were the result of alterations in lysosomal pH, Lee et al. (2010) used a LysoSensor yellow/blue DND-160–Dextran probe to reveal that WT cells displayed an average lysosomal pH of 4.7 ± 0.08, while PS1ko blastocysts displayed a substantially elevated lysosomal pH of 5.4 ± 0.04. We attempted to reproduce the findings of Lee et al. (2010) using an unconjugated pH-dependent fluorescent probe, LysoSensor DND-160 that interrogates the pH of all intracellular organelles, and is not specific to lysosomes. We generated a standard curve by obtaining images of cultured WT-ES cells, at both blue (W1) and yellow (W2) wavelengths, which were incubated in MES buffer clamped at various pH values (pH7.5–3.5). The pH-sensitive nature of the dual emission probe is clearly seen in Figure 2*A*, and the W1/W2 ratios (Fig. 2*B*) allowed us to generate a standard curve (Fig. 2*C*). We then incubated cultured WT-ES, PS1ko-ES, and PSdko-ES cells with the Lysosensor-DND-160 dye and obtained pseudo-colored images (Fig. 2*D*) from which we quantified the W1/W2 ratio distribution of a population of vesicles in each cell line (Fig. 2*E*). Converting the W1/W2 ratio to vesicle pH revealed that the mean vesicle pH for cultured WT-ES and PS1ko-ES cells (Fig. 2*G*) are not significantly different, but that there is significant increase in the population of vesicles with lower pH values in cultured PSdko-ES cells (Fig. 2*F*). While the mechanism(s) have yet to be determined by which PS deficiency decreases overall intracellular vesicle pH in cultured PSdko-ES cells, our studies in cultured PS1ko-ES cells fail to confirm the results of Lee et al. (2010) that showed an acidification defect in PS1ko blastocysts.

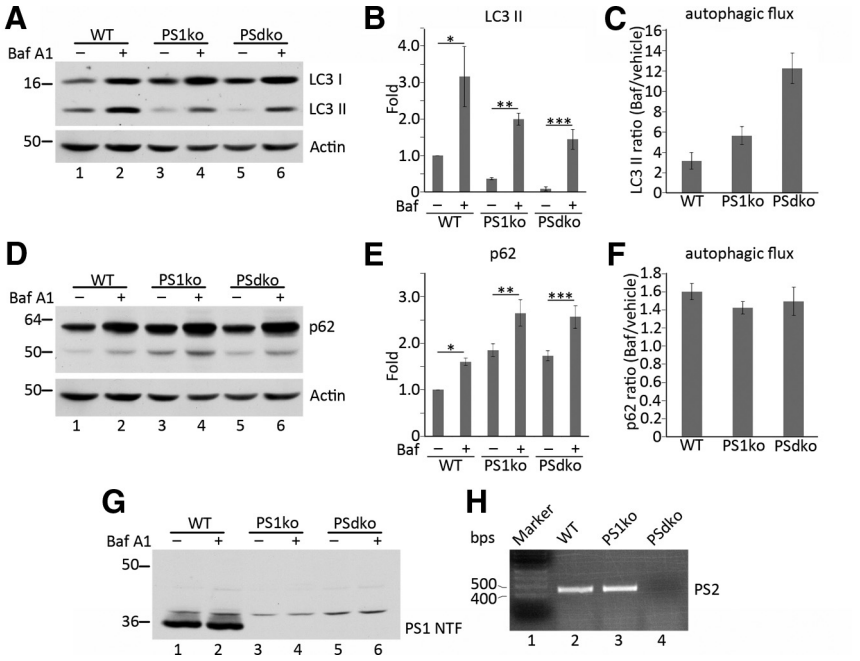

Figure 1. Quantification of LC3 and p62 levels in the presence or absence of bafilomycin A1 in cultured WT-ES, PS1ko-ES, and PSdko-ES Cells. ***A***, LC3 levels detected by Western blotting. ***B***, Quantification of LC3 II levels normalized to actin ($*p < 0.06$, $**p < 0.01$, $***p < 0.05$, $n = 3$). ***C***, Autophagic flux of LC3II in WT-ES, PS1ko-ES, and PSdko-ES cells. ***D***, p62 levels detected by Western blotting. ***E***, Quantification of p62 levels normalized to actin ($*p < 0.01$, $**p < 0.01$, $***p < 0.05$, $n = 5$). ***F***, Autophagic flux of p62 in WT-ES, PS1ko-ES, and PSdko-ES cells. ***G***, Detection of PS1 expression in WT-ES, PS1ko-ES, and PSdko-ES cells. ***H***, Detection of PS2 expression by RT-PCR in WT-ES, PS1ko-ES, and PSdko-ES cells.

Processing of cathepsin D is not impaired in cultured PS1ko-ES and PSdko-ES cells or in brains of mice lacking PS in excitatory neurons

In view of the reported deficits in lysosomal acidification, Lee et al. (2010) examined the proteolytic maturation of the lysosomal hydrolase, cathepsin D (CatD). It is well established that pro-CatD is transported from the Golgi complex to acidic endolysosomal compartments where the propeptide is removed to generate an active ~48 kDa intermediate that is further processed into an ~14 kDa N terminal light chain and an ~34 kDa C-terminal heavy chain (Zaidi et al., 2008). Western blot studies by Lee et al. (2010) revealed that in PS1ko blastocysts, the steady-state ~48 kDa intermediate accumulated to high levels, while the ~34 kDa and ~14 kDa chains of CatD were significantly reduced compared with those in WT blastocysts, wherein the levels of the processed derivatives were prominent. These findings lead the authors to conclude that lysosome-specific functions necessary for CatD processing were impaired in PS1ko cells. In view of our failure to demonstrate any alteration in lysosomal pH in cultured PS1ko-ES and PSdko-ES cells, we reexamined CatD processing in these cells and in cultured WT-ES cells. In contrast to the results reported by Lee et al. (2010), we now show that the steady-state levels of either the ~48 kDa intermediate form or the ~34 kDa heavy chain of CatD in detergent lysates of cultured WT-ES, PS1ko-ES, and PSdko-ES cells are indistinguishable (Fig. 3*A*, lanes 1–3).

It should be noted that the steady-state levels of the ~52 pro-CatD and ~48 kDa intermediate forms of CatD in lysates from cultured PS1ko-ES and PSdko-ES cells are elevated compared with the levels of these CatD derivatives in cultured WT-ES cells (Fig. 3*A*). Our earlier microarray studies of the hippocampus and cortex from PScdko mouse brain (see below) revealed an age-dependent elevation in mRNA encoding CatD that was accompanied by an increase in the steady-state levels of the ~48 and ~34 kDa CatD-related polypeptides (Mirnics et al., 2008). To assess the possibility that the elevated levels of CatD protein in the cultured PS1ko-ES and PSdko-ES cells were a reflection of changes in CatD mRNA, we prepared total RNA from cultured WT-ES, PS1ko-ES, and PSdko-ES cells and quantified the steady-state levels of mRNA encoding CatD. We failed to observe any differences in transcripts encoding CatD between the cultured ES cells (Fig. 3*B*, $p > 0.05$). Supporting this conclusion, transcriptomic analysis of WT-ES cells and PS1ko and PSdko ES cells failed to reveal an elevation of CatD transcripts in the PS1ko and PSdko ES cells (ctsd; see Table 2). Hence, the mechanism(s) that regu-

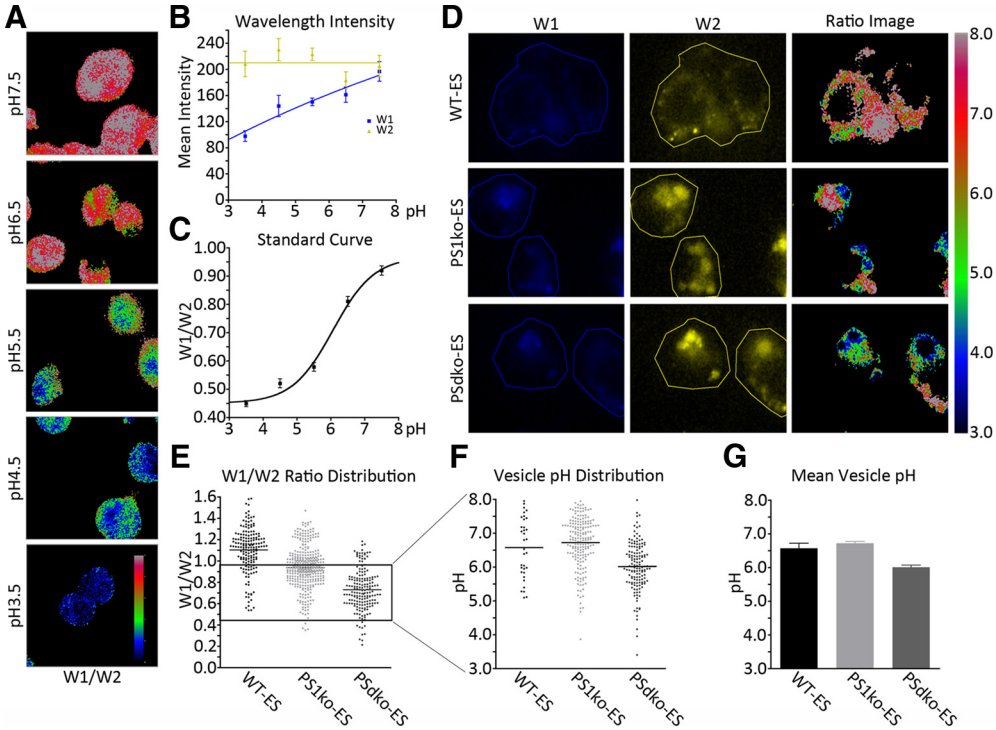

Figure 2. Mean vesicle pH measurement in cultured WT-ES, PS1ko-ES, and PSdko-ES Cells. ***A***, Representative images of cultured WT-ES cells used for ratiometric analysis using the pH-sensitive probe Lysosensor-DND-160. Images were collected while ES cells were incubated in buffer clamped at various pH values (pH7.5, 6.5, 5.5, 4.5, and 3.5). ImageJ was used to generate a ratiometric image where pH is represented by a color following the scale (in ***B***). ***B***, Graph showing the pH-sensitive nature of the dual emission probe, Lysosensor-DND-160, at acidic pH for blue (W1), but not yellow (W2), emission spectra ($N = 10$); two-way ANOVA: $p < 0.0001$ ($F = 74.64$, $DF_{n=4,d=58}$), post-tests: W1 versus W2; pH 7.5 ($p > 0.05$), pH 6.0 ($p < 0.01$), pH 5.0, 4.5, and 4.0 ($p < 0.001$), values are mean ± SEM. ***C***, Graph showing the standard curve (ratio = W1/W2, $N = 20$ vesicles/pH, values are mean ± SEM). ***D***, Pseudo colored images of cultured WT-ES, PS1ko-ES, and PSdko-ES cells incubated with the Lysosensor-DND-160 dye. Fifteen 60× images were collected per group and the experiment was repeated twice. The number of cells in each encircled "field" varied both within and between ES cell types because of differences in cell size and morphology. ***E***, W1/W2 ratio distribution of all vesicles in each ES cell type. ***F***, Vesicle pH distribution within the acidic range in WT-ES, PS1ko-ES, and PSdko-ES cells. ***G***, Mean vesicle pH in WT-ES, PS1ko-ES, and PSdko-ES cells within the acidic range.

lates the apparent increase in steady-state levels of CatD in PS1ko-ES and PSdko-ES cells remains to be determined.

Finally, we assessed CatD processing in the brains of $PS1^{lox/lox}/PS2^{-/-}/cre$ mice (hereafter referred to as PScdko mice). To generate the PScdko mice, we crossed "floxed" *PSEN1* mice ($PS1^{lox/lox}$ mice), wherein endogenous *PSEN1* harbors internal loxP sites, to *PSEN2*-deficient mice ($PS2^{-/-}$) mice. Mice homozygous at both loci were crossed with mice expressing cre recombinase driven by the *α-CaMKII-cre* that is only active postnatally in excitatory neurons, and subsequently backcrossed to generate mice that lack expression of *PSEN1* in excitatory neurons and *PSEN2* throughout the neuraxis and in peripheral tissues. Earlier studies have reported that these PScdko mice exhibit age-associated neurodegeneration throughout the forebrain after the age of 5–6 months (Saura et al., 2004; Chen et al., 2008). Indeed, Lee et al. (2010) used ultrastructural approaches to reveal that the brains of these animals exhibited abnormally elevated levels of LC3-positive vesicles, and decreased acidification of lysosomal compartments, findings that were interpreted to suggest that *PSEN* deficiency impairs autophagolysosomal function in an *in vivo* setting. We now show that while the steady-state levels of CatD are elevated in PScdko hippocampus, as previously reported (Mirnics et al., 2008), the patterns of CatD-related polypeptides in lysates from the hippocampi of PScdko mice and control littermates are indistinguishable (Fig. 3*C*, lanes 1 and 2). We confirmed that PS1 expression was largely eliminated in brains of PScdko mice (Fig. 3*C*, lane 2), leading to the hyperaccumulation of APP-CTFs (Fig. 3*C*, lane 2).

Glycosylation of the V0a1 subunit of V-ATPase is not regulated by PS

In view of the acidification defects observed in PS1ko blastocysts, Lee et al. (2010) examined the subcellular distribution and glycosylation of the V0a1 subunit of the vacuolar ATPase (V-ATPase) that is essential for proton translocation and lysosomal acidification. The authors reported that in contrast to WT cells, V0a1 was primarily localized to the endoplasmic reticulum and depleted from lysosomal compartments in PS1ko cells. Consistent with these findings, Western blot analysis revealed that while WT cells expressed both ~100 kDa immature/unglycosylated species and endo H-resistant ~120 kDa V0a1-related species, V0a1 failed to mature in PS1ko cells, resulting in the accumulation of endo H-insensitive ~100 kDa species.

Our initial attempts to detect V0a1 with a commercially available antibody disclosed extremely low, albeit detectable, levels of this subunit in lysates of MEF or ES cells (data not shown). Thus, we generated a brain-specific human V0a1 cDNA (Nishi and Forgac, 2000) with a myc-6xHis epitope tag at its C terminus (V0a1–6His), and examined the maturation of the encoded polypeptide in transfected MEF or ES cells. We stably expressed V0a1–6His in cultured WT or PSdko MEF cells and examined the glycosylation status of the ectopically expressed V0a1–6His. Surprisingly, we observed that the pattern and levels of ~110 kDa and ~120–140 kDa human V0a1–6His-related polypeptides in cultured WT and PSdko MEF cells were indistinguishable (Fig. 4*A*, compare lanes 1 and 4), and, in both cases, the ~120–140 kDa species were equally susceptible to digestion with PNGase F,

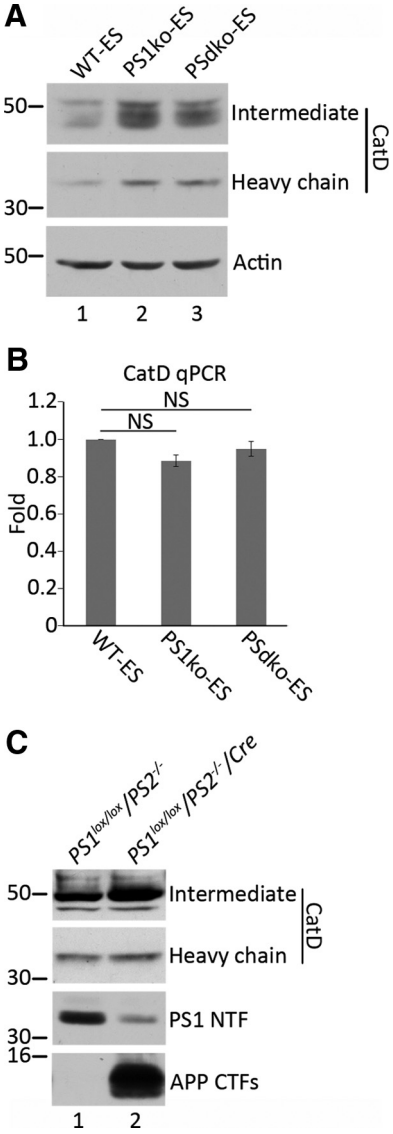

Figure 3. Processing of cathepsin D in the absence of presenilin(s). ***A***, Processing of cathepsin D in cultured WT-ES, PS1ko-ES, and PSdko-ES cells. Intermediate and heavy chain of CatD are shown in the upper two panels, respectively; actin is used as an internal loading control. ***B***, Quantification of cathepsin D expression by quantitative PCR analysis in cultured WT-ES, PS1ko-ES, and PSdko-ES cells. The results represent the mean ± SEM of four sets of reactions for each ES cell type ($p > 0.07$ and $p > 0.3$ respectively, $n = 4$). NS, Nonsignificant. ***C***, Cathepsin D processing in PScdko mice. Intermediate and heavy chain of CatD are shown in the top two panels and PS1 NTF and APP CTFs levels are shown in the bottom panels.

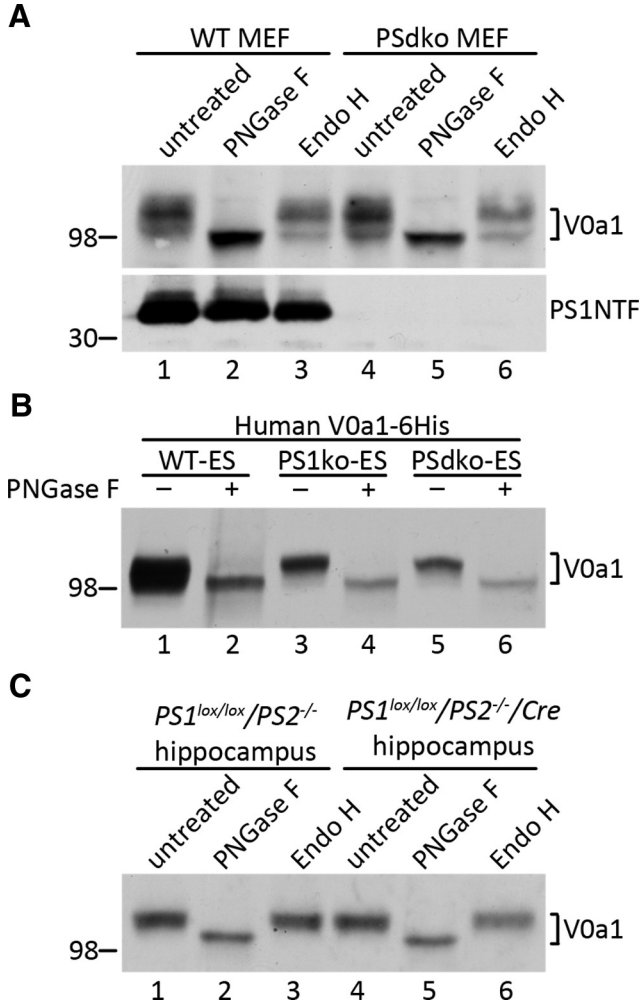

Figure 4. V0a1 is glycosylated in the absence of presenilin(s). ***A***, Stably expressed human V0a1–6His is glycosylated in cultured PSdko MEF. The treatment of the lysates with PNGase F or Endo H is indicated above lanes 2, 3, 5, and 6. The respective presence and absence of PS1 expression in cultured WT and PSdko MEF is shown in the bottom panel. ***B***, Transiently expressed human V0a1–6His is glycosylated in the absence of presenilin(s) in ES cells. PNGase F treatment is indicated above lanes 2, 4, and 6. ***C***, Endogenous V0a1 is glycosylated in the hippocampi of PScdko mice. The treatment with PNGase F or EndoH is indicated above lanes 2, 3, 5, and 6, respectively.

an amidase that cleaves between the innermost GlcNAc and asparagine residues of high mannose, hybrid, and complex oligosaccharides, resulting in the generation of an ~100 kDa species (Fig. 4*A*, lanes 2 and 5). The fact that the ~120–140 kDa V0a1–6His species remained resistant to digestion with endo H, an endoglycosidase that cleaves asparagine-linked mannose-rich oligosaccharides, but not highly processed complex oligosaccharides (Fig. 4*A*, compare lanes 3 and 6), suggests that V0a1–6His polypeptides have acquired hybrid and/or complex oligosaccharides in WT MEF cells and MEF cells that lack both *PSEN1* and *PSEN2*.

To validate these findings in ES cells, we transiently transfected cDNA encoding human V0a1–6His into cultured WT-ES, PS1ko-ES, and PSdko-ES cells. Although the levels of accumulated V0a1 in each cell line varied, this was due to differences in transient transfection efficiencies; using a GFP reporter assay, we estimated the transient transfection efficiencies of WT-ES, PS1ko-ES, and PSdko-ES cells to be between 30 and 50%, 20 and 30%, and 10 and 20%, respectively. Western blot analysis revealed that as in cultured WT-ES cells, transiently expressed human V0a1–6His in cultured PS1ko-ES and PSdko-ES cells acquired mixed and/or complex oligosaccharides (Fig. 4*B*, lanes 1, 3, 5). Collectively, our studies in both MEFs and ES cells reveal that the absence of *PSEN1* expression either singly, or in combination with *PSEN2*, has no impact on oligosaccharide maturation of V0a1, findings that fail to confirm the findings of Lee et al. (2010).

Finally, we examined the glycosylation of endogenous V0a1 in brains of PScdko mice. We now show that in PScdko ($PS1^{lox/lox}/PS2^{-/-}/Cre$) mice, mouse V0a1 acquires hybrid and/or complex oligosaccharides (Fig. 4*C*, lanes 4–6), compared with littermate control $PS1^{lox/lox}/PS2^{-/-}$ mice in which *α-CaMKII-cre* is not expressed, but in which only the *PSEN2* gene is disrupted (Fig. 4*C*,

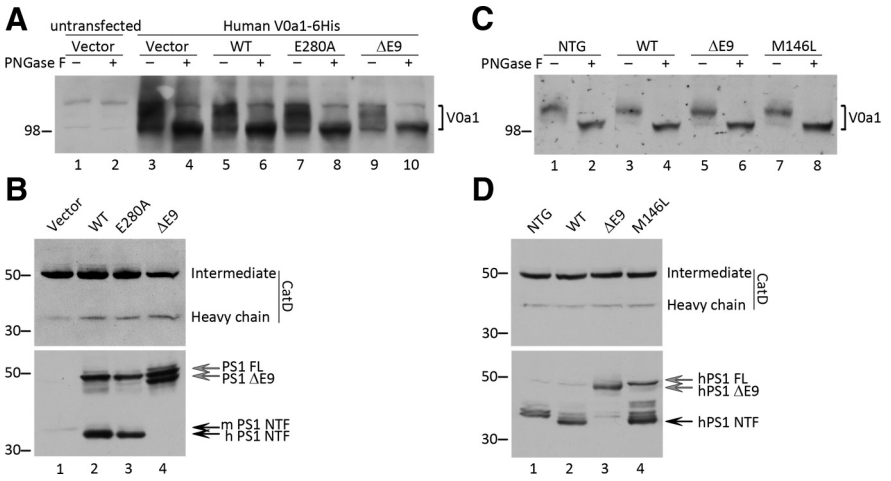

Figure 5. V0a1 is glycosylated and cathepsin D is processed into mature forms in cells and brains of mice expressing independent FAD-linked mutant PS1. ***A***, Human V0a1–6His is glycosylated in N2a cells stably expressing FAD-linked PS1 mutants E280A and ΔE9. V0a1–6His was transiently transfected into N2a cells harboring human PS1 or FAD-linked mutant E280A or ΔE9. Untransfected or empty vector-transfected cells were used as controls (lanes 1–4). PNGase F treatment is indicated above the lanes. ***B***, Cathepsin D is processed into mature forms in N2a cells stably expressing FAD-linked PS1 mutants E280A and ΔE9. Levels of both intermediate form and heavy chain of CatD are shown in the top panel. The expression of human PS1 and FAD-linked E280A and ΔE9 are shown in the bottom panel. Full-length human PS1 and unproteolysed ΔE9 are indicated by gray arrows; endogenous mouse PS1NTF is indicated by a black arrow labeled with m, and the human PS1 NTF is indicated by a black arrow labeled with h. ***C***, Endogenous V0a1 is glycosylated in the brains of transgenic mice overexpressing either wild-type human PS1, or FAD-linked PS1 ΔE9 or PS1 M146L; non-transgenic (NTG) littermate is also used as a control. Treatment with PNGase F is indicated above the corresponding lanes. ***D***, Cathepsin D is processed into mature forms in an indistinguishable pattern in non-transgenic brain, or in transgenic brains overexpressing WT human PS1, or FAD-linked PS1ΔE9 or PS1M146L. The expression of human PS1, or FAD-linked PS1ΔE9 or M146L is shown in the bottom, full-length human PS1 and unproteolysed PS1ΔE9 are indicated by gray arrows; human PS1 NTF is indicated by a black arrow.

lanes 1–3). It should be noted that in PScdko mice, *α-CaMKII-cre*-mediated disruption of endogenous *PSEN1* is incomplete (Fig. 3*C*, compare PS1 NTF in lanes 1 and 2); our estimate is that <10% of PS1 remains after *PSEN1* disruption specifically in excitatory neurons (for quantification, see Fig. 6*A*, compare lanes 11 and 14). Thus, it might be argued that this residual level may have been sufficient to support maturation of V0a1 in PScdko mice, despite the fact that the levels of full-length PS1 are essentially undetectable (see Fig. 6*A*, below). Moreover, we have shown that in the PScdko mice at 6 months of age, *PSEN1* is fully deleted in neurons within the CA fields and granule cells within the hippocampus (Feng et al., 2001). In this regard, it is well established that *PSEN1* expression is not restricted to excitatory neurons (Lee et al., 1996; Sherrington et al., 1995; Lah et al., 1997), and hence, we would suggest that the residual PS1 signal observed in these studies is a reflection of expression in interneurons and non-neuronal cells. More importantly, and in view of the fact that the total levels of V0a1 in WT and PScdko mice are comparable, we find it inconceivable that the levels of mature V0a1 in the PScdko mice represent expression in those cells wherein *PSEN1* remains intact.

Analysis of V0a1 maturation and CatD processing in transgenic mice and neuroblastoma N2a cells expressing WT and FAD-linked PS1 variants

Lee et al. (2010) extended their studies of PS1ko blastocysts to examine the impact of expressing FAD-linked PS1 variants (PS1-FAD) on autophagy. The authors reported that degradation of long-lived proteins in several of PS1-FAD fibroblast cell lines that express independent PS1 variants was lower compared with that in control cells, and that in one FAD-PS1 fibroblast line, both the LC3-II/LC3-I ratio and total LC3-II levels were higher than that observed in control fibroblasts. Furthermore, LysoTracker staining revealed that lysosomal pH in one PS1-FAD fibroblast line was substantially higher than control fibroblasts. To assess the possibility that the acidification deficits could be attributed to defective maturation of V0a1, the authors reported that in contrast to control fibroblasts in which V0a1 colocalized with CatD-positive compartments, very little V0a1 colocalized with CatD in PS1 FAD fibroblasts, but instead colocalized with an ER-resident protein, protein disulfide isomerase (PDI). Additional biochemical studies on a single FAD-PS1 fibroblast line showed decreased levels of maturation of V0a1 compared with those in control fibroblasts. Thus, Lee et al. (2010) concluded that "cells expressing FAD-linked PS1 display a similar loss of lysosomal function as in PS1ko cells that might account for the marked acceleration of autophagy-related dysfunction and neuronal cell death associated with PS1-FAD."

In an attempt to validate these findings, we examined V0a1 maturation and CatD processing in stable N2a cell lines that express independent FAD-linked PS1 variants and in brains of transgenic mice that express either human WT PS1 or two FAD-linked variants in a ubiquitous manner. For the former, we transiently transfected stable N2a "pools" expressing either human PS1, or the FAD-linked A280E or ΔE9 variants with cDNA encoding human V0a1–6His (see above), and examined the expression and maturation of the ectopically expressed protein (Fig. 5*A*). In contrast to the report by Lee et al. (2010) that revealed a defect in maturation of V0a1 in a single FAD-PS1 fibroblast line, we failed to demonstrate that oligosaccharide maturation of the expressed V0a1 in N2a cells that express either the A280E or ΔE9 variants (Fig. 5*A*, lanes 7 and 8; 9 and 10, respectively) is any different from that observed in cells expressing WT PS1 (Fig. 5*A*, lanes 5 and 6). Extending these findings, we assessed CatD maturation in the stable N2a cell "pools" as a surrogate marker for lysosomal acidification and function. Western blot analysis revealed that the steady-state levels of the intermediate and heavy chains of CatD were identical between cells that express either PS1 or the FAD-linked A280E and PS1ΔE9 PS1 variants (Fig. 5*B*, compare lanes 2, 3, 4, respectively). Finally, we used PS1NT antibody to confirm stable expression of PS1 and FAD-linked variants in the stable N2a cell pools (Fig. 5*B*, bottom). These studies reveal that endogenous PS1 (Fig. 5*B*, lane 1; arrowhead) is subject to "replacement" by exogenous human PS1 (Fig. 5*B*, lanes 2–4) as a result of competition for limiting, endogenous components of the γ-secretase complex (nicastrin, Aph-1 and PEN-2), as we described previously (Thinakaran et al., 1996, 1997). Notably, while full-length human PS1 is apparent in the WT and A280E pools, these species are known to be rapidly degraded (Thinakaran et al., 1997; Ratovitski et al., 1997). The effect on replacement is most obvious for cells expressing the PS1ΔE9 variant (Fig. 5*B*, lane 4) that fails to undergo endoproteolytic processing due to deletion of a region that contains the endoproteolysis site, but nevertheless competes

for limiting factors in the γ-secretase complex (Thinakaran et al., 1996; Lee et al., 1997).

Finally, we examined V0a1 maturation in the brains of mice that express mouse prion promoter-driven transgenes encoding either human WT PS1 (Thinakaran et al., 1996) or the FAD-linked M146L or ΔE9 variants (Lee et al., 1997). These studies document that the maturation of V0a1 in brains of mice that express either human PS1 or FAD-linked PS1 polypeptides in a ubiquitous manner is indistinguishable (Fig. 5*C*, compare lanes 3, 4 to lanes 5, 6 and 7, 8). Extending these experiments, we examined the maturation of CatD in the brains of our transgenic mouse lines. As we observed in the N2a cell lines, the levels of CatD-related intermediate and heavy chains were indistinguishable in brain extracts from mice expressing either human PS1 or the FAD-linked M146L or ΔE9 variants (Fig. 5*D*, compare lanes 2–4, respectively). Finally, we confirmed the expression of PS1 and FAD-linked variants in the transgenic mouse lines and the replacement of endogenous PS1 (Fig. 5*D* bottom, lanes 2–4), as we had previously documented (Thinakaran et al., 1997). Collectively, our studies reveal that expression of FAD-linked PS1 variants either in stable cell lines or in the brains of transgenic mice neither impairs the glycosylation of V0a1, nor the maturation of CatD and hence, fail to support the conclusions by Lee et al. (2010) that cells expressing FAD-linked PS1 exhibit a loss of lysosomal function.

Mechanistic analysis of PS1-mediated regulation of V0a1 maturation

Using coimmunoprecipitation approaches, Lee et al. (2010) reported that full-length PS1 associated with the immature, unglycosylated form of V0a1 and a subunit of the oligosaccharyltransferase (OST) complex, termed STTB, that is involved in posttranslational glycosylation of selected substrates. From these findings, the authors proposed that full-length PS1 serves as a chaperone to assist in posttranslational glycosylation of V0a1; in the absence of PS1, V0a1 fails to acquire oligosaccharide modifications, and thus, does not exit from the endoplasmic reticulum and is subsequently degraded. As a consequence of failed maturation and targeting of V0a1 to lysosomal compartments, lysosomal pH is elevated, leading to impaired autophagosomal function. We were perplexed by these findings because we (Thinakaran et al., 1996, 1997; Ratovitski et al., 1997; Lee et al., 1996) and others (Podlisny et al., 1997) have reported that in untransfected cells, murine tissues, and human and monkey brain, PS1 and PS2 accumulate as ~30 kDa N-terminal (NTF) and ~20 kDa C-terminal (CTF) derivatives at steady-state, and that full-length PS1 and PS2 are virtually undetectable. Confirming these latter findings, we performed Western blots of detergent-solubilized extracts from cultured WT and PSdko MEF (Fig. 6*A*, lanes 1–5), cultured WT-ES and PSdko-ES cells (Fig. 6*A*, lanes 6–10), or from hippocampi from $PS1^{lox/lox}/PS2^{-/-}$ and PScdko mice (Fig. 6*A*, lanes 11–14) using anti-PS1NT antibody raised against the intracellular N-terminal domain of PS1. We show that full-length PS1 is detectable, albeit at extremely low levels in lysates prepared from cultured WT MEF and WT-ES cells, but is virtually absent in extracts prepared from mouse hippocampus.

In view of the inherent difficulty of detecting full-length PS1 in mammalian cells or in brain, we used two alternative approaches to test the model that full-length PS1 interacts with V0a1 and STT3B. In the first, we stably expressed V0a1–6His in a HEK293 cell line that constitutively expresses a short hairpin (sh) duplex designed to target mRNA encoding PEN-2 (Prokop et al., 2004). In the PEN-2 knockdown (PEN2KD) line, the level of PEN-2, a subunit of the γ-secretase complex that is essential for PS endoproteolysis and "activation" of the enzyme (Ahn et al., 2010), is markedly reduced (Fig. 6*B*, compare lanes 1 and 2), leading to accumulation of full-length PS1 (Fig. 6*B*, lane 2). Using anti-6xHis antibodies to immunoprecipitate exogenous V0a1 and associated proteins, we failed to recover full-length PS1 or PS1-NTFs (Fig. 6*C*, lane 3). Similarly, α-PS1NT failed to coimmunoprecipitate V0a1–6His (Fig. 6*C*, lane 3′), under conditions in which this antibody successfully recovered endogenous NCT, a subunit of the γ-secretase complex (Fig. 6*C*, lane 3″). We then asked whether full-length PS1 interacts with the OST subunit, STT3B. Using anti-STT3B antibodies, we failed to recover full-length PS1 or PS1-NTFs (Fig. 6*D*, top, lane 3), under conditions in which the antibody successfully coimmunoprecipitated OST48, an established subunit of the OST enzyme complex (Fig. 6*D*, bottom, lane 3). Reverse-coimmunoprecipitation studies using anti-PS1NT antibody failed to coimmunoprecipitate STT3B (Fig. 6*D*, lane 3′), under conditions wherein this antibody recovered both full-length PS1 and PS1 derivatives (Fig. 6*D*, lanes 3′). Collectively, our studies fail to demonstrate an association of full-length PS1 with either V0a1 or STT3B.

While these latter studies failed to reveal an interaction of STT3B or V0a1 with full-length PS1 in PEN2KD cells, it was conceivable that in these cells, the association of full-length PS1 with nicastrin and APH-1 in the "preactivation" complex (Takasugi et al., 2003) might hinder potential interactions with STT3B or V0a1. To address this possibility, our second strategy was to employ a stable N2a cell line that overexpresses human WT PS1 (Borchelt et al., 1996). In these cells, Western blot analysis of detergent lysates reveals that full-length PS1 is detectable, but is relatively unstable (Ratovitski et al., 1997). We now show that in N2aWT PS1 cells, full-length PS1 is not recovered with either anti-STT3B or anti-V0a1 antibodies (Fig. 6*E*, lanes 5, 6) to levels any higher than found using normal IgG (Fig. 6*E*, lane 4), while anti-PS1 antibodies efficiently immunoprecipitate both full-length PS1 and PS1 NTF (Fig. 6*E*, lane 7). Hence, in two independent settings, namely, PEN2KD cells and cells overexpressing PS1, we fail to document the association of PS1 with V0a1 or STT3B.

A model proposed by Lee et al. (2010) is that full-length PS1 regulates the maturation of V0a1 by holding it in proximity to STT3B, and thereby facilitates posttranslational glycosylation of the substrate. To examine the role of STT3B in glycosylation of V0a1, we transfected HEK293 cells with V0a1–6His and treated these cells with siRNAs that selectively target the two principal OST subunits that are critical for cotranslational (STT3A) or posttranslational glycosylation (STT3B) of glycoproteins (Ruiz-Canada et al., 2009).

We find that treatment with siRNA specific to each subunit selectively and effectively blocks synthesis of the respective target proteins (Fig. 7*A*, panel STT3A, lanes 4, 5; panel STT3B, lanes 6, 7). More importantly, we observe that the maturation of prosaposin (PSAP), a polypeptide that is selectively glycosylated by STT3A, is significantly impaired in cells lacking STT3A (Fig. 7*A*, panel PSAP, lanes 4, 5). Similarly, the maturation of procathepsin C (proCatC), a STT3B-specific substrate, is also diminished in cells lacking STT3B (Fig. 7*A*, panel pCatC, lanes 5, 6). Notably, procathepsin C is difficult to detect by Western blotting because proCatC, like CatD, is proteolytically processed in the lysosome. Interestingly, we failed to detect any effects on the maturation of V0a1–6His by reducing the levels of either STT3A or STT3B in these cells (Fig. 7*A*, panel V0a1, lanes 4–7). We then considered the possibility that V0a1 might be long-lived, hence masking the

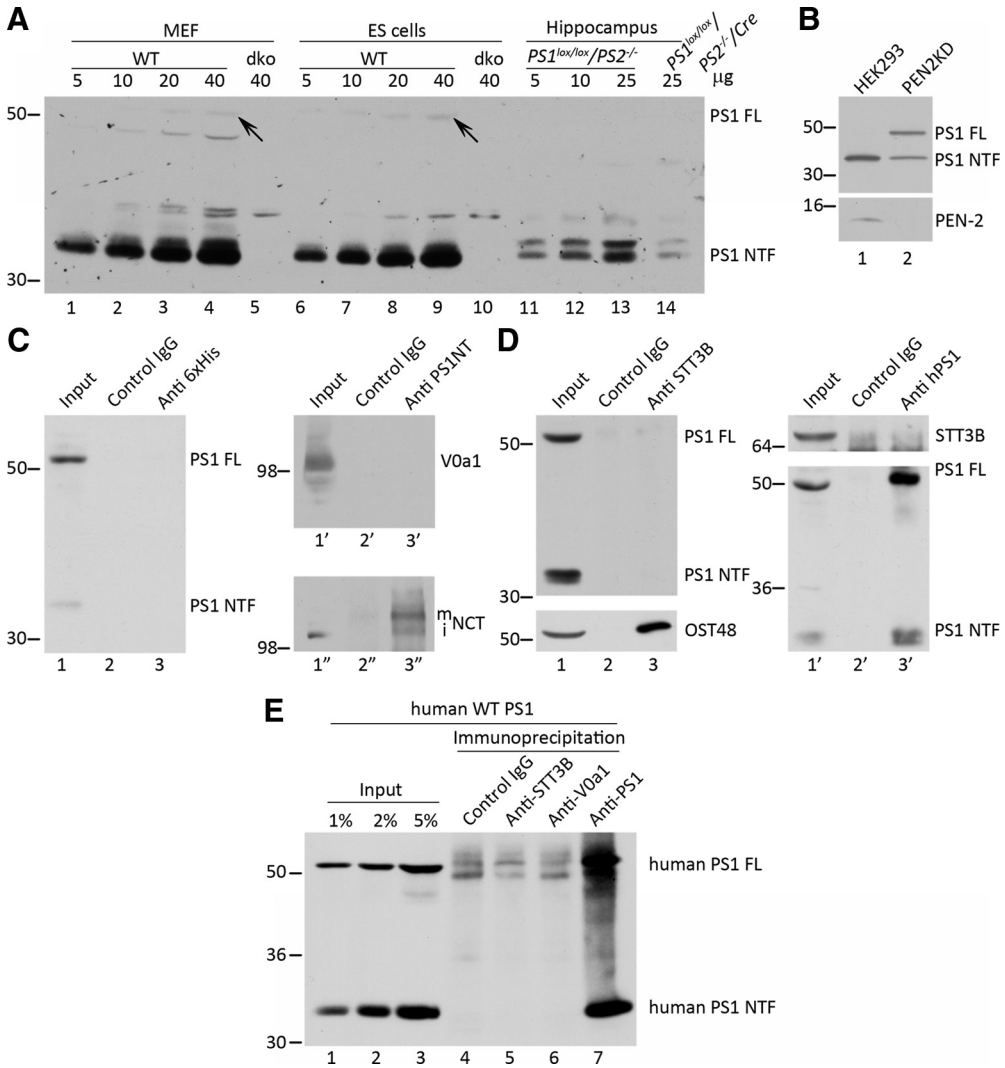

Figure 6. Full-length PS1 does not coimmunoprecipitate with V0a1 or STT3B. ***A***, A series of diluted lysates of cultured WT MEF and WT-ES cells or mouse hippocampi are used to assess the levels of full-length PS1 and PS1 NTF. Very low level of full-length PS1 is detected in MEF and ES cell lysates, while no full-length PS1 is detected in hippocampus lysates under these conditions. Full-length PS1 is indicated by an arrow. ***B***, PEN-2 knockdown cell line (PEN2KD) reveals the accumulation full-length PS1 compared with naive HEK 293 cells. The level of the remaining PEN-2 in this cell line is shown in the bottom when naive HEK293 cell lysate is used as a control. ***C***, No co-immunoprecipitation of full-length PS1 or PS1NTF with V0a1–6His is detected in PEN-2 knockdown cells (left panel with anti-6XHis antibody, right top panel with anti-PS1NT antibody), while under the same conditions the co-immunoprecipitation of PS1 and NCT was confirmed (right bottom panel). m, Mature nicastrin band; i, immature nicastrin band. ***D***, No co-immunoprecipitation of full-length PS1 and STT3B is detected (left top panel with anti-STT3B antibody, right top panel with anti-human PS1 antibody), while under the same conditions the co-immunoprecipitation of STT3B and OST48 is confirmed (left bottom panel), and the immunoprecipitated full-lengthPS1 and PS1 NTF are shown in the right bottom panel. ***E***, With lysates from mouse N2a cells stably expressing human WT PS1, coimmunoprecipitation was performed with control IgG, anti-STT3B, and anti-V0a1 antibodies. Anti-PS1 was used as a control for the immunoprecipitation. The immunoprecipitated samples were probed with anti-human PS1 antibody. No specific interaction between full-length PS1 with either STT3B or V0a1 was detected.

effects of lowering STT3A or STT3B on newly synthesized V0a1. Hence, we chose to perform pulse-labeling and immunoprecipitation studies to examine the levels and glycosylation of newly synthesized V0a1–6His. In this case, we observe that siRNA-mediated reduction of STT3B levels has very little impact on the maturation of V0a1–6His, but surprisingly, reduction of STT3A levels leads to a profound and reproducible elevation in the mature forms of V0a1–6His. It is not presently clear whether this is the result of an elevation in STT3B levels in cells in which STT3A is diminished (Fig. 7*B*, panel STT3B, lanes 3, 4). However, we previously showed that depletion of STT3A does not fully eliminate cotranslational glycosylation, a finding that led us to conclude that the STT3B isoform has cotranslational access to skipped glycosylation sites (Ruiz-Canada et al., 2009), and, hence, it is conceivable that the increased level of newly synthesized V0a1–6His might be the result of STT3B-dependent glycosylation of V0a1 that would otherwise be modified by STT3A. Indeed, analysis of single knockdowns of STT3A or STT3B revealed that certain glycoproteins like ribophorin I were not hypoglycosylated, and that three of the four glycosylation sites in proCatC can be cotranslationally modified by either STT3A or STT3B. These data, together with our results, indicate that the glycosylation site in V0a1 can be glycosylated by both the STT3A and STT3B isoforms of the OST.

Expression of genes associated with autophagy is not altered in cultured PS1ko-ES and PSdko-ES cells and brains of adult mice that lack PS in excitatory neurons

Our studies have revealed that the absence of expression of *PSEN1* alone, or in combination with *PSEN2*, does not influence the autophagolysosomal turnover of LC3-II or p62. To gain a

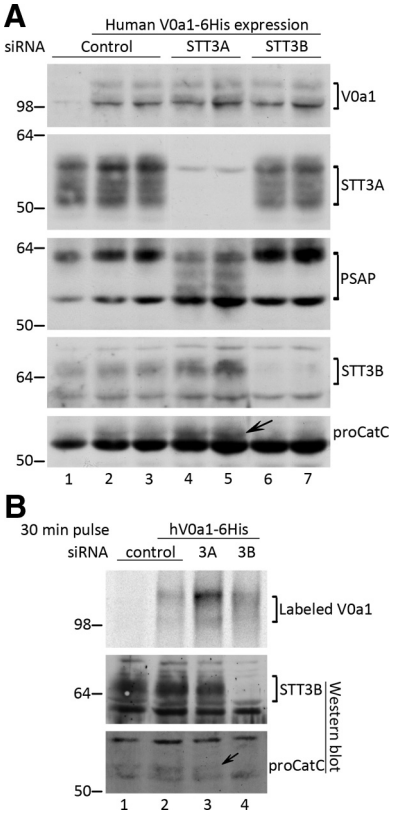

Figure 7. V0a1 is glycosylated when either STT3A or STT3B is downregulated in HEK 293 Cells. ***A***, HEK 293 cells were transfected with control siRNA (lanes 1–3), STT3A siRNA (lanes 4 and 5), or STT3B siRNA (lanes 6 and 7) followed by a transient transfection with V0a1–6His cDNA. V0a1 panel shows the expression and the glycosylation state of V0a1 in these transfected cells. STT3A panel confirms the depletion of STT3A following the STT3A siRNA transfection (lanes 4 and 5). PSAP panel shows the selective reduction of the glycosylation of a STT3A substrate PSAP (lanes 4 and 5), which further confirms the loss of STT3A activity following STT3A siRNA transfection. STT3B panel confirms the depletion of STT3B following the STT3B siRNA transfection (lanes 6 and 7). The proCatC panel shows the selective reduction of the glycosylation of a STT3B substrate procathepsin C (lanes 6 and 7), which further confirms the loss of STT3B activity following STT3B siRNA treatment. ***B***, Pulse-labeling of HEK293 cells cotransfected with V0a1– 6His and either control siRNA, STT3A, or STT3B siRNA, and cells transfected with control siRNA alone was used as a control for V0a1– 6His immunoprecipitation. Labeled V0a1 panel shows the level and glycosylation state of labeled V0a1 after immunoprecipitation with anti-6XHis antibody under each condition. STT3B and proCatC panels show the Western blot results of the labeled samples to confirm the depletion of STT3B following the STT3B siRNA transfection (STT3B panel, lane 4) and the reduction of proCatC glycosylation after STT3B siRNA treatment (proCatC panel lane 4). proCatC band is indicated with an arrow.

more global assessment of autophagic activity, we chose to examine the transcription of genes associated with autophagy using two approaches. First, we asked whether the expression of a recently described master transcriptional regulator of lysosomal biogenesis and autophagy, termed TFEB (Settembre et al., 2011), is altered in cultured PSdko MEF or ES cells compared with corresponding WT cells. The rationale for this study is that transient overexpression or siRNA-mediated suppression of TFEB level leads to elevated or suppressed expression of TFEB target genes, respectively (Settembre et al., 2011). Real-time PCR analysis failed to reveal a statistically significant difference in levels of transcripts encoding TFEB in cultured PSdko MEFs or ES cells compared with WT counterparts (Fig. 8*A*; $\Delta\Delta C_T = -0.1$, $p > 0.2$), findings which strongly argued against a defect in the expression of genes that are controlled by this transcriptional regulator of the autophagic pathway in *PSEN*-deficient cells. To validate these findings, we then assessed transcriptome profiles in cultured WT-ES, PS1ko-ES, and PSdko-ES cells using high density oligonucleotide arrays, paying particular attention to the expression of a set of genes that have been recently reported (Settembre et al., 2011) to be direct targets of TFEB, a transcription factor that binds a consensus palindromic 10-base pair (bp) GTCACGTGAC motif, as well as genes that belong to autophagy machinery components, including *UVRAG*, *WIPI*, *MAPLC3B*, *SQSTM1*, *VPS11*, *VPS18*, *ATG9B*, *AMBRA1*, *ATG12*, *ATG16L1*, *ATG4A*, *ATG4B*, *ATG4C*, *ATG4D*, *ATG5*, *ATG9A*, *BECN1*, *GABARAP*, *GABARAPL1*, *GABARAPL2*, *IRGM*, *MAP1LC3A*, *RGS19*, and *ULK1*. As a gene group, these transcripts showed no significant enrichment compared with overall distribution of transcripts (mean $ALR_{PSdko\text{-}CNT} = -0.13$; $p = 0.267$) (Table 1), and only the mRNA encoding *ATG9B* showed a marked increase in expression in the cultured PS1ko-ES (SKO) and PSdko-ES (DKO) cells compared with WT-ES cells (218% and 65%, respectively). Thus, with the exception of *ATG9B*, there does not appear to be a general alteration in expression of TFEB-target autophagy machinery components. In parallel to the analysis of TFEB target genes that are involved in autophagy and autophagy machinery component genes, we assessed TFEB target genes that are critical for lysosomal biogenesis. These genes belong to the CLEAR network (Sardiello et al., 2009). Compared with the overall distribution of average log ratios between the cultured PSdko-ES and WT-ES cells, TFEB target genes that are critical for lysosomal biogenesis showed a populational shift that was significant (mean $ALR_{PSdko\text{-}CNT} = -0.24$; $p = 0.00013$). Of these, we observed a greater than two-fold downregulation of *ACP5*, *CTSF*, *CTSH*, *GGH*, and *LIPA* transcripts (Table 2). This suggested that compound deficiency of *PSEN1* and *PSEN2* is affecting the expression of genes related to lysosomal biogenesis, and hence, we sought to confirm this hypothesis in an *in vivo* model.

To this end, we examined the transcriptome profiles in the frontal cortex and hippocampi of PScdko mice. We first confirmed the selective expression of *cre* recombinase in mature excitatory neurons by crossing the *α-CaMKII-cre* transgenic mice (line T29-1) with *Gt[ROSA]26Sor*$^{tm4[ACTB\text{-}tdTomato,\text{-}EGFP]Luo}$ mice (Muzumdar et al., 2007), which harbor a knockin cassette within the mouse ROSA26 locus. The knockin cassette contains *loxP* sites on either side of sequences encoding a membrane-targeted tdTomato [mTomato red] cassette upstream of sequences encoding a membrane-targeted EGFP [mEGFP] (Fig. 8*B*). Constitutive expression of mTomato red results in strong red fluorescence in all brain regions and cell types (Fig. 8*B*). When bred to *α-CaMKII-cre* mice, the resulting offspring have the mTomato red cassette deleted in the cells expressing *cre* recombinase, thus activating expression of mEGFP (Fig. 8*B*). Examination of 5-week-old bigenic mice carrying both *α-CaMKII-cre* and *ROSA26* reporter transgenes revealed the expression of mEGFP, a direct read out of *cre* recombinase activity, throughout the cortex and hippocampus (Fig. 8*Ci*). In contrast, the single transgenic *Gt[ROSA]26Sor*$^{tm4[ACTB\text{-}tdTomato,\text{-}EGFP]Luo}$ mice brain sections showed uniform mTomato red expression (Fig. 8*Cii*), with no detectable mEGFP expression (Fig. 8*Ciii*). Compared with the single transgenic *Gt[ROSA]26Sor*$^{tm4[ACTB\text{-}tdTomato,\text{-}EGFP]Luo}$ line, no gross changes in anatomical regions of the brain were observed in bigenic mice. Furthermore, confocal imaging revealed that the morphology of mEGFP positive cells in bigenic mice resemble mature granule cell neurons of the dentate gyrus (Fig. 8*Civ*), pyramidal cell neurons in CA1 (Fig. 8*Cviii*), mossy fibers in CA3 (Fig. 8*Cxii*), and neurons in all layers of cortex (Fig.

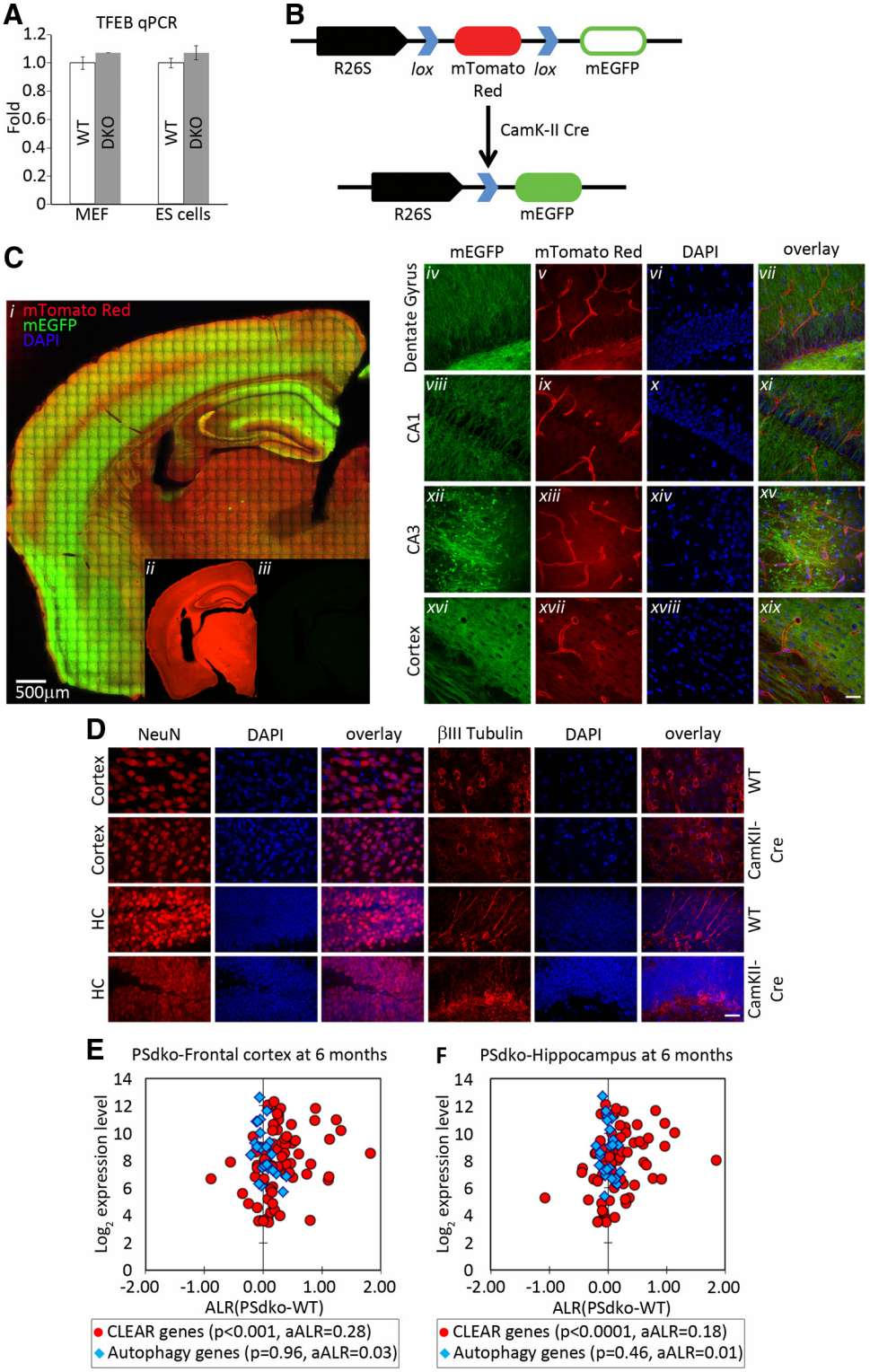

Figure 8. Expression of genes associated with autophagy and lysosomal biogenesis in cells and mouse brain. ***A***, Quantitative PCR analysis of TFEB expression in WT and PSdko MEF and ES cells. The results represent the mean ±SEM of four sets of reactions for each cell type ($p > 0.2$, $n = 4$). ***B***, Strategy to assess α-*CaMKII* promoter driven *cre* recombinase activity *in vivo*. Expression of α-*CaMKII-cre* leads to excision of loxP sites flanking mTomato red coding region and thereby activating mEGFP reporter expression within the ROSA26 locus [R26S]. ***Ci***, Photograph of montage created by confocal *z*-stack tiled image of coronal brain section (×40 obj) from bigenic mice carrying CaMKII-*cre* and *Gt[ROSA]26Sor*$^{tm4[ACTB-tdTomato,-EGFP]Luo}$ transgenes; overlay of mEGFP (green), mTomato red (red), DAPI (blue) is shown; scale bar, 500 μm. ***Cii***, ***Ciii***, Representative photographs of coronal brain section from single transgenic *Gt[ROSA]26Sor*$^{tm4[ACTB-tdTomato,-EGFP]Luo}$ mice show expression of mTomato red (***Cii***), without detectable mEGFP signal (***Ciii***). ***Civ–Cxix***, Confocal *z*-stack projection images (×40 obj) of cells expressing mEGFP or mTomato red in specific hippocampal subfields and cortex of bigenic mice are shown in columns ***Civ*** to ***Cxiv*** and ***Cv*** to ***Cxvii***, respectively. DAPI stained nuclei (column ***Cvi*** to ***Cxviii***) and the overlay (column ***Cvii*** to ***Cxix***) of mEGFP, mTomato red, and DAPI signal are shown. Scale bar, 100 μm. ***D***, Neuronal morphology in WT and CaMKII promoter-driven cre recombinase mice. Cortical or hippocampal sections from brains from WT and CaMKII-cre mice were stained with antibodies to the nuclear antigen, NeuN or the cytoskeletal antigen, βIII tubulin. Scale bar, 100 μm. ***E***, ***F***, Transcriptome analysis of mouse FC and HC, respectively. In both figures, autophagy genes are in blue diamonds and CLEAR network genes in red circles. *x*-axis denotes average log2 ratio (ALR) for each gene (1 ALR = 2-fold change); *y*-axis corresponds to normalized log2 expression value observed on the DNA microarray (denoting the magnitude of the expression level of a gene). Differential expression values of the (*Figure legend continues.*)

Table 1. Differential expression of autophagy genes in PSdko, PS1ko, and WT ES cells

Gene symbol	WT	SKO	DKO	ALR SKO-WT	ALR DKO-WT
Uvrag	9.77	9.73	9.55	−0.05	−0.23
Wipi1	8.51	8.56	8.00	0.05	−0.51
Sqstm1	11.36	11.46	11.13	0.10	−0.23
Vps11	8.63	8.58	8.13	−0.05	−0.50
Vps18	8.81	8.43	8.35	−0.37	−0.46
Atg9b	4.65	6.33	5.38	1.67	0.73
Ambra1	8.34	8.69	8.87	0.35	0.54
Atg12	8.18	8.09	8.26	−0.09	0.08
Atg16l1	9.61	9.08	9.15	−0.53	−0.46
Atg4a	8.83	8.80	8.27	−0.03	−0.56
Atg4b	9.59	9.61	9.39	0.01	−0.21
Atg4c	6.75	6.98	7.09	0.22	0.34
Atg4d	7.76	8.08	8.07	0.33	0.31
Atg5	8.82	8.87	8.82	0.05	−0.01
Atg9a	8.32	8.62	8.35	0.30	0.03
Becn1	10.21	10.45	9.92	0.24	−0.29
Gabarap	12.05	12.09	11.58	0.05	−0.47
Gabarapl1	10.74	10.53	10.03	−0.21	−0.70
Gabarapl2	11.35	11.22	11.24	−0.13	−0.11
Irgm1	5.02	5.62	5.59	0.60	0.57
Map1lc3a	11.60	11.08	11.22	−0.52	−0.38
Rgs19	10.05	9.84	10.39	−0.20	0.34
Ulk1	8.84	8.44	8.13	−0.40	−0.71
Average ALR				0.06	−0.13
p value				0.506	0.266

8*Cxvi*). Importantly, no detectable *cre*-induced mEGFP expression is observed in non-neuronal cell types, including vascular endothelium that was positive for mTomato red (Fig. 8*Cv*, *ix*, *xiii*, *xvii*). These data confirm that *cre* recombinase activity in the bigenic mice is specific to postmitotic, excitatory neurons, without activity in other CNS cell types.

Finally, in view of studies which have reported that *cre* recombinase can promote recombination at cryptic sites (Semprini et al., 2007; Thyagarajan et al., 2000) and that high levels of *cre* expression driven by a nestin promoter in neuronal progenitors causes defects in proliferation, aneuploidy, and cell death (Forni et al., 2006), we compared the neuronal cell morphology and nuclear architecture in WT mice and in mice that express CaMKII promoter-driven *cre* recombinase. We observed neither cellular nor nuclear alterations in neurons in the hippocampus or cortex of mice expressing *CaMKII-cre* (Fig. 8*D*).

In our earlier efforts, we reported that mice with compound deficiencies of *PSEN1* and *PSEN2* in excitatory neurons lead to a progressive, age-dependent transcriptome signature related to neurodegeneration and neuroinflammation (Mirnics et al., 2008). Reexamination of this dataset failed to uncover a change in the expression of either TFEB, or any TFEB target genes associated with autophagy or other autophagy-related genes (Table 3). However, there was a clear and highly significant elevation in the expression of the lysosomal biogenesis CLEAR network genes in both the fontal cortex (FC) and hippocampus (HC) of 6-month-old PScdko mice compared with littermate $PS1^{lox/lox}/PS2^{-/-}$ mice con-

←

(*Figure legend continued.*) TFEB-dependent autophagy genes and CLEAR network genes in the HC and FC can be found in Table 3. Note that in both the frontal cortex and hippocampus the CLEAR network genes showed a highly significant groupwise overexpression (FC: $p = 2.0*10^{-19}$; HC: $p = 6.6*10^{-9}$), while the TFEB-dependent autophagy-related genes showed no populational expression shift (FC: $p = 0.96$; HC: $p = 0.46$). The most overexpressed genes of the CLEAR network in both the FC and HC included: *Ctsd*, *Naglu*, *Gusb*, *Ctsz*, *Ctss*, *Hexb*, and *Cd68*.

Table 2. Differential expression of CLEAR network genes in PSdko, PS1ko, and WT ES cells

Gene symbol	WT	AVG SKO	AVG DKO	ALR SKO-WT	ALR DKO-WT
Abca2	5.31	5.23	5.12	−0.07	−0.19
Abcb9	5.08	4.96	4.87	−0.13	−0.21
Cd68	6.71	6.65	6.37	−0.06	−0.33
Cln3	8.71	8.66	8.73	−0.05	0.03
Laptm4a	12.49	12.41	12.48	−0.08	−0.01
Lamp3/Ppid	11.76	11.66	11.89	−0.10	0.13
Litaf	11.54	11.47	11.84	−0.07	0.29
Lamp1	12.72	12.55	12.39	−0.17	−0.33
Lamp2	11.32	11.08	10.46	−0.23	−0.86
Mfsd8	6.88	6.74	6.89	−0.14	0.01
Mcoln2	4.86	4.18	4.12	−0.67	−0.73
Mcoln1	10.03	10.39	9.81	0.36	−0.22
Mcoln3	4.33	4.37	4.37	0.04	0.04
Ncstn	9.44	9.43	9.26	−0.01	−0.18
Npc1	8.56	8.21	7.81	−0.36	−0.75
Npc1l1	4.88	4.52	4.69	−0.36	−0.19
Cenpc1	9.38	9.32	9.54	−0.06	0.16
Slc17a2	4.42	4.84	4.68	0.42	0.26
Slc17a6	4.55	4.41	4.36	−0.14	−0.19
Slc17a1	4.41	4.06	4.31	−0.35	−0.11
Slc17a7	4.02	4.01	3.96	−0.01	−0.06
Slc17a5	8.80	8.88	8.39	0.08	−0.40
Slc17a3	4.24	4.40	4.16	0.17	−0.08
Slc17a9	5.89	5.83	6.21	−0.06	0.32
Lipa	10.02	8.85	8.28	−1.17	−1.73
Gla	9.29	9.29	9.00	0.00	−0.29
Naglu	8.23	9.05	8.22	0.82	0.00
Arsb	6.81	9.05	4.99	2.24	−1.82
Arsa	9.61	9.67	9.18	0.07	−0.43
Glb1	9.74	9.52	9.14	−0.22	−0.61
Gusb	7.09	4.32	8.76	−2.77	1.68
Hexb	9.98	9.72	9.18	−0.26	−0.80
Manba	9.54	9.73	9.69	0.19	0.15
Cpvl	5.12	5.06	5.31	−0.06	0.19
Ctsb	12.24	12.21	12.23	−0.03	−0.01
Ctsd	11.92	11.66	11.31	−0.26	−0.60
Ctsf	9.42	9.00	8.00	−0.42	−1.42
Ctsh	12.06	11.52	10.31	−0.55	−1.75
Ctsk	5.98	6.10	5.88	0.13	−0.09
Ctsl	13.05	12.87	12.82	−0.18	−0.23
Ctso	4.85	4.79	4.97	−0.06	0.12
Ctss	4.06	4.71	4.60	0.65	0.54
Ctsz	11.34	11.63	11.50	0.29	0.16
Cln5	9.49	9.65	9.45	0.17	−0.03
Dnase2a	6.00	6.10	6.30	0.09	0.29
Ggh	9.02	8.47	6.34	−0.54	−2.67
Gm2a	9.46	9.75	8.80	0.29	−0.66
Mgea5	11.12	11.42	10.83	0.30	−0.29
Ids	9.76	9.65	9.47	−0.11	−0.29
Ifi30	11.46	11.74	11.93	0.27	0.46
Lgmn	12.88	12.65	12.26	−0.23	−0.61
Ganab	11.08	10.86	10.45	−0.22	−0.63
Ctsa	11.45	10.76	10.71	−0.69	−0.74
Mpo	4.28	4.13	4.29	−0.15	0.01
Galns	8.46	8.42	8.32	−0.04	−0.14
Gns	11.66	11.09	11.21	−0.57	−0.45
Npc2	12.57	12.37	12.46	−0.20	−0.11
Npc1	8.56	8.21	7.81	−0.36	−0.75
Ppt1	9.74	9.60	9.24	−0.14	−0.50
Ppt2	9.56	9.33	9.77	−0.23	0.21
Psap	11.58	11.51	11.39	−0.07	−0.19
Siae	8.21	8.33	8.18	0.12	−0.03
Neu1	10.59	10.50	9.69	−0.10	−0.91
Smpd1	6.75	6.05	9.70	−0.70	2.95
Fuca1	9.33	10.07	9.54	0.75	0.21
Tpp1	11.80	11.63	11.28	−0.17	−0.52
Acp2	8.99	8.42	8.59	−0.57	−0.41
Acp5	9.26	7.66	6.96	−1.60	−2.30
Average ALR				−0.10	−0.24
p value				0.10170167	0.00012541

Table 3. Differential expression of TFEB-dependent autophagy and lysosomal biogenesis (CLEAR) genes in the brain of 6-month-old PSdko mice

CLEAR genes			Autophagy genes		
Gene symbol	ALR 6 mos FC KO-WT	ALR 6 mos HC KO-WT	Gene symbol	ALR 6 mos FC KO-WT	ALR 6 mos HC KO-WT
Abca2	0.17	0.15	*Atg12*	0.04	−0.03
Abcb9	−0.10	−0.04	*Atg16l1*	−0.13	0.15
Cd68	1.82	1.84	*Atg4a*	0.16	−0.02
Cln3	0.37	−0.09	*Atg4b*	−0.13	−0.21
Laptm4a	0.08	−0.12	*Atg4c*	−0.04	0.23
Laptm4b	0.26	−0.04	*Atg4d*	0.04	0.09
Lamp3/ Ppid	−0.12	−0.22	*Atg5*	−0.14	−0.01
Litaf	0.61	−0.04	*Atg9a*	−0.20	−0.14
Lamp1	0.27	0.09	*Atg9b*	−0.05	0.34
Lamp2	0.49	0.60	*Becn1*	0.09	0.11
Mfsd8	−0.13	−0.24	*Gabarapl1*	−0.09	−0.06
Mcoln2	0.08	−0.06	*Gabarapl2*	−0.01	−0.11
Mcoln3	0.79	−0.16	*Gabarap*	0.07	−0.05
Mcoln1	−0.05	−0.20	*Map1lc3b*	−0.01	−0.09
Ncstn	0.02	0.11	*Map1lc3a*	−0.03	0.07
Npc1	0.13	−0.06	*Rgs19*	−0.07	0.03
Npc1l1	−0.25	0.03	*Ulk1*	0.18	0.06
Cenpc1	0.00	0.13	*Atg10*	0.22	0.17
Slc17a2	0.09	−0.34	*Atg16l2*	0.13	−0.07
Slc17a6	−0.56	−0.44	*Atg3*	0.04	−0.04
Slc17a6	−0.89	−1.07	*Atg7*	0.07	0.40
Slc17a1	0.09	−0.03	*Atg7*	0.00	0.07
Slc17a7	0.26	0.11	*Rab24*	0.08	−0.10
Slc17a5	0.47	0.17	Autophagy Mean	0.01	0.03
Slc17a3	−0.08	0.12	*p* value	0.96	0.46
Lipa	0.05	0.04			
Gla	−0.35	0.36			
Naga	0.38	0.06			
Naglu	1.11	0.77			
Arsb	0.23	0.30			
Arsa	0.25	0.19			
Glb1	0.25	0.61			
Gusb	1.11	0.91			
Hexb	1.31	1.14			
Manba	0.16	0.10			
Cpvl	−0.10	−0.11			
Ctsb	0.30	0.26			
Ctsd	0.88	0.81			
Ctsf	0.04	−0.04			
Ctsh	0.81	0.65			
Ctsk	0.01	−0.18			
Ctsl	0.47	0.31			
Ctso	0.32	−0.10			
Ctss	1.24	0.97			
Ctsz	1.13	0.97			
Cln5	0.50	0.15			
Dnase2b	0.00	−0.18			
Dnase2a	0.12	0.27			
Ggh	0.45	0.11			
Gm2a	0.38	0.45			
Gm2a	0.14	−0.44			
Mgea5	0.23	0.07			
Ids	0.13	−0.08			
Ids	0.08	0.13			
Ifi30	0.74	0.22			
Lgmn	0.37	0.55			
Ganab	0.06	0.02			
Ctsa	0.55	0.69			
Mpo	0.19	0.31			
Galns	0.15	0.45			
Gns	0.39	0.21			
Npc2	0.88	0.50			
Ppt1	−0.17	−0.13			
Ppt2	0.02	0.13			
Psap	0.19	−0.05			
Siae	−0.11	0.06			
Neu1	0.02	0.21			
Neu1	0.16	0.29			
Smpd1	0.17	0.21			
Fuca1	0.36	0.24			
Tpp1	0.15	0.06			
Acp2	0.32	0.33			
Acp5	0.28	−0.10			
CLEAR Mean	0.28	0.18			
p value	0.001	0.001			

(*Table continues.*)

trols (Fig. 8*E*,*F*) (FC: $p = 2.0^{*}10^{-19}$; HC: $p = 6.6^{*}10^{-9}$). The most overexpressed genes in the lysosomal biogenesis network in both the FC and HC included: *CTSD*, *NAGLU*, *GUSB*, *CTSZ*, *CTSS*, *HEXB*, and *CD68*.

Thus, in both cultured PS1ko-ES and PSdko-ES cells and brains of PScdko mice, we failed to observe significant alterations in the expression of TFEB target genes involved in autophagy. However, in brains of PScdko mice, we found evidence of altered expression of the genes involved in lysosomal biogenesis, defined as the CLEAR network (Sardiello et al., 2009).

Discussion

The accumulation of autophagic vacuoles is a consistent feature of many neurodegenerative diseases (Shintani and Klionsky, 2004). The significance of the described perturbations in the autophagic pathways in Alzheimer's disease gained support by a report by Lee et al. (2010), in which the authors concluded that the absence of *PSEN1* expression impaired the clearance of autophagosomes during macroautophagy due to a selective impairment in lysosomal acidification. These deficits were attributed to failed association of PS1 holoprotein with STT3B and V0a1, and defects in posttranslational glycosylation and targeting of the V0a1 to lysosomes. Moreover, human fibroblasts expressing FAD-linked PS1 variants also exhibited lysosomal/autophagy deficits similar to cells lacking PS1.

In view of the provocative outcomes reported by Lee et al. (2010), we reexamined several aspects of the model and now offer several insights that collectively fail to support the conclusions drawn by the authors. First, we document that while LC3-II levels are considerably diminished in cultured PSdko-ES cells compared with WT-ES cells, autophagic flux assays reveal that this is the result of an active autophagic pathway in cells lacking *PSEN*.

Second, we demonstrate that the mean vesicle pH in cultured PS1ko-ES cells and WT-ES cells is essentially identical, but the vesicle pH in PSdko-ES cells exhibits a shift toward more acidic pH values. The mechanism(s) underlying this observation remains to be determined, but Neely et al. (2011) recently showed that vesicle acidification was unchanged in MEFs lacking *PSEN* compared with WT MEFs. Third, we show that proteolytic processing of CatD is indistinguishable in cultured WT-ES, PS1ko-ES, and PSdko-ES cells. Furthermore, we show that CatD processing in hippocampi from PScdko mice and littermate controls are identical. As the dissociation of CatD from mannose 6-phosphate receptors in lysosomes requires acidic pH and CatD processing is mediated by proteases with acidic pH optima, we would infer that the absence of *PSEN* has no significant influence on lysosomal pH. Fourth,

we demonstrate that N-linked glycosylation of V0a1 in MEFs or ES cells that lack *PSEN* is indistinguishable from corresponding WT cells. We confirmed this result by showing that the maturation of V0a1 in the hippocampi of PScdko mice is identical to that in their littermate controls. Hence, these results are entirely consistent with our observation that lysosomal pH and function is unimpaired in the absence of *PSEN*. Fifth, we failed to observe any differences in N-linked glycosylation of V0a1 and CatD processing in N2a cells or in brains of mice expressing WT or FAD-linked PS1 variants, findings that fail to support the studies reported by Lee et al. (2010). Sixth, we examined the association of PS1 holoprotein with V0a1 and/or STT3B. In this regard, we document that PS1 holoprotein is essentially undetectable at steady-state in both cells and brain; we estimate that the endoproteolytic derivatives of PS1 accumulate to ~0.0025% of total brain protein (Thinakaran et al., 1996). Hence, we chose to use PEN-2 knockdown cell line (Prokop et al., 2004), which has an elevated steady-state level of PS1 holoprotein, or stable N2a cells that overexpress WT human PS1. In neither of these cell lines did we find an association of PS1 holoprotein with either V0a1 or STT3B. Finally, we asked whether V0a1 is a substrate for N-linked glycosylation by STT3B. Indeed, we were intrigued by the model proposed by Lee et al. (2010) because the 834–856 aa mouse V0a1 isoforms harbor a single lumenally exposed potential N-linked glycosylation site (asparagine 489) (Nishi and Forgac, 2000; Leng et al., 1999). However, we have shown that N-linked sites that serve as STT3B substrates are generally found at either N- or C-terminal regions of the polypeptide backbone (Ruiz-Canada et al., 2009). When tested in cells wherein STT3A or STT3B was depleted, we failed to confirm that V0a1 is uniquely glycosylated by STT3B.

In summary, we now report that cells lacking expression of PS1 either singly, or in combination with PS2 exhibit robust autophagy, and that the loss of PS function neither alters intracellular pH, N-linked glycosylation of V0a1, or processing of CatD. Finally, we fail to confirm the association of PS1 holoprotein with either V0a1 or STT3B. How can we reconcile these findings with those reported by Lee et al. (2010)? We speculate that the PS1ko blastocysts, from which the bulk of the data were obtained by Lee et al. that revealed deficits in autophagy, elevated lysosomal pH, inefficient glycosylation of V0a1, and CatD processing, are, in some manner, compromised, perhaps as a consequence of issues related to clonal drift and/or compensation. In this regard, we found it curious that a series of "rescue" experiments intended to demonstrate that human PS1 can reverse the reported phenotypes in PS1ko blastocysts were not conducted in the PS1ko blastocysts, but inexplicably, were performed in PSdko blastocysts. Lee et al. (2010) reported that human PS1 fully "rescues" the deficits in protein degradation, vesicle acidification, macroautophagy responses, V0a1 maturation, and CatD processing that existed in PS1ko cells. What was conspicuously absent in this dataset was information pertaining to the aforementioned biological outcomes in naive PSdko cells, particularly in view of the findings reported herein that failed to reveal a deficit in any of these processes in these cells.

To these latter insights, we assessed the expression of TFEB and genes involved in autophagy, and now report no differences in TFEB mRNA between cultured PSdko-ES and WT-ES cells. Moreover, transcriptome analysis of cultured PS1ko-ES and PSdko-ES cells failed to reveal any significant alteration in the expression of autophagy-specific genes. However, *ATG9B* expression was elevated in both the cultured PS1ko-ES and PSdko-ES cells, but it is presently unclear as the function of this phagophore/pre-autophagosomal structure (PAS) (Suzuki et al., 2001; Yen and Klionsky, 2007) associated polytopic membrane protein has not been established. Similarly, transcriptome analysis of PScdko mice failed to uncover any alterations in the expression of TFEB or genes involved in autophagy. Meanwhile, we show a significant elevation in CLEAR network genes in the FC and HC of 6-month-old PScdko mice compared with littermate controls. In contrast, we observed a small, but significant decrease in the populational expression of CLEAR network genes in cultured PS1ko-ES and PSdko-ES cells compared with WT-ES cells. Moreover, with the exception of elevated *CTSS* transcript levels, the CLEAR gene expression changes between PSko-ES cells and PScdko brains do not overlap. While these latter results would seem conflicting, we would argue that the observed differences represent cell type-specific mechanisms that lead to elevated lysosomal function. ES cells are clonal, proliferative, pluripotent stem cells, and the response of these cells to *PSEN* deficiency may be significantly different from that observed in the brains of PScdko mice in which *PSEN1* is selectively ablated in postmitotic, excitatory neurons. In this regard, while we observe an elevation in steady-state levels of CatD in extracts from PS1ko and PSdko ES cells, this is not due to an increase in *CatD* mRNA (Fig. 3*A*,*B*). In contrast, both CatD mRNA and protein are elevated in brains of PScdko mice (Mirnics et al., 2008) (Fig. 3*C*, Table 3). It is instructive that the basal, steady-state levels of the autophagy substrate, LC3-II, are lower in PS1ko and PSdko ES cells compared with WT ES cells, a finding which would suggest that lysosomal hydrolase activity is elevated, leading to enhanced turnover of this substrate in the absence of PS. Indeed, in PS1ko and PSdko cells treated with bafilomycin, the levels of LC3-II are markedly elevated, and autophagic flux is strongly enhanced. Hence, it is conceivable that in PS1ko and PSdko cells, the steady-state levels or catalytic activity of other lysosomal proteases are also elevated without corresponding increases in the mRNAs encoding these polypeptides. This hypothesis remains to be tested.

The mechanism(s) by which loss of *PSEN* expression elicits an increase in the expression of CLEAR genes in PScdko brains is not fully understood. However, we would offer the tentative proposal that in the absence of PS/γ-secretase activity, the membrane-tethered stubs derived from type 1 membrane proteins that would normally be processed by γ-secretase in endosomal, late Golgi compartments or the plasma membrane would now accumulate in lysosomal compartments wherein the proteases critical for lysosomal function would be "saturated." As a result, excitatory neurons lacking *PSEN* expression would respond by inducing CLEAR genes as a compensatory mechanism. We should note that in addition to scoring expression in excitatory neurons, CLEAR gene expression in the PScdko brains is the summation of expression patterns in inhibitory interneurons, microglia, astrocytes, pericytes, and endothelial cells. Moreover, and in view of the fact that astroglial activation is associated with neurodegeneration in 6-month-old PScdko brain, other gene expression changes will certainly contribute to the transcriptome.

In any event, the fact that all the genes in the CLEAR network contain TFEB-binding site(s), and that TFEB mRNA levels are not impacted by the expression of PS, we can only conclude that in mouse brain, PS regulates pathway(s) critical for lysosomal biogenesis, but in a TFEB mRNA expression-independent manner. The mechanism(s) that underlies this unanticipated, but novel aspect of PS biology remains to be investigated.

References

Ahn K, Shelton CC, Tian Y, Zhang X, Gilchrist ML, Sisodia SS, Li YM (2010) Activation and intrinsic gamma-secretase activity of presenilin 1. Proc Natl Acad Sci U S A 107:21435–21440.

Borchelt DR, Thinakaran G, Eckman CB, Lee MK, Davenport F, Ratovitsky T, Prada CM, Kim G, Seekins S, Yager D, Slunt HH, Wang R, Seeger M, Levey AI, Gandy SE, Copeland NG, Jenkins NA, Price DL, Younkin SG, Sisodia SS (1996) Familial Alzheimer's disease-linked presenilin 1 variants elevate Abeta1-42/1-40 ratio in vitro and in vivo. Neuron 17:1005–1013.

Chen Q, Nakajima A, Choi SH, Xiong X, Sisodia SS, Tang YP (2008) Adult neurogenesis is functionally associated with AD-like neurodegeneration. Neurobiol Dis 29:316–326.

Choi SH, Veeraraghavalu K, Lazarov O, Marler S, Ransohoff RM, Ramirez JM, Sisodia SS (2008) Non-cell-autonomous effects of presenilin 1 variants on enrichment-mediated hippocampal progenitor cell proliferation and differentiation. Neuron 59:568–580.

De Strooper B (2003) Aph-1, Pen-2, and Nicastrin with Presenilin generate an active gamma-Secretase complex. Neuron 38:9–12.

De Strooper B, Annaert W (2010) Novel research horizons for presenilins and gamma-secretases in cell biology and disease. Annu Rev Cell Dev Biol 26:235–260.

Feng R, Rampon C, Tang YP, Shrom D, Jin J, Kyin M, Sopher B, Miller MW, Ware CB, Martin GM, Kim SH, Langdon RB, Sisodia SS, Tsien JZ (2001) Deficient neurogenesis in forebrain-specific presenilin-1 knockout mice is associated with reduced clearance of hippocampal memory traces. Neuron 32:911–926.

Forni PE, Scuoppo C, Imayoshi I, Taulli R, Dastrù W, Sala V, Betz UA, Muzzi P, Martinuzzi D, Vercelli AE, Kageyama R, Ponzetto C (2006) High levels of Cre expression in neuronal progenitors cause defects in brain development leading to microencephaly and hydrocephaly. J Neurosci 26:9593–9602.

Hu S, Delorme N, Liu Z, Liu T, Velasco-Gonzalez C, Garai J, Pullikuth A, Koochekpour S (2010) Prosaposin down-modulation decreases metastatic prostate cancer cell adhesion, migration, and invasion. Mol Cancer 9:30.

Ichimura Y, Kominami E, Tanaka K, Komatsu M (2008) Selective turnover of p62/A170/SQSTM1 by autophagy. Autophagy 4:1063–1066.

Kabeya Y, Mizushima N, Ueno T, Yamamoto A, Kirisako T, Noda T, Kominami E, Ohsumi Y, Yoshimori T (2000) LC3, a mammalian homologue of yeast Apg8p, is localized in autophagosome membranes after processing. EMBO J 19:5720–5728.

Kim SH, Sisodia SS (2005) Evidence that the "NF" motif in transmembrane domain 4 of presenilin 1 is critical for binding with PEN-2. J Biol Chem 280:41953–41966.

Klionsky DJ, Elazar Z, Seglen PO, Rubinsztein DC (2008) Does bafilomycin A1 block the fusion of autophagosomes with lysosomes? Autophagy 4:849–950.

Lah JJ, Heilman CJ, Nash NR, Rees HD, Yi H, Counts SE, Levey AI (1997) Light and electron microscopic localization of presenilin-1 in primate brain. J Neurosci 17:1971–1980.

Lee JH, Yu WH, Kumar A, Lee S, Mohan PS, Peterhoff CM, Wolfe DM, Martinez-Vicente M, Massey AC, Sovak G, Uchiyama Y, Westaway D, Cuervo AM, Nixon RA (2010) Lysosomal proteolysis and autophagy require presenilin 1 and are disrupted by Alzheimer-related PS1 mutations. Cell 141:1146–1158.

Lee MK, Slunt HH, Martin LJ, Thinakaran G, Kim G, Gandy SE, Seeger M, Koo E, Price DL, Sisodia SS (1996) Expression of presenilin 1 and 2 (PS1 and PS2) in human and murine tissues. J Neurosci 16:7513–7525.

Lee MK, Borchelt DR, Kim G, Thinakaran G, Slunt HH, Ratovitski T, Martin LJ, Kittur A, Gandy S, Levey AI, Jenkins N, Copeland N, Price DL, Sisodia SS (1997) Hyperaccumulation of FAD-linked presenilin 1 variants in vivo. Nat Med 3:756–760.

Leng XH, Nishi T, Forgac M (1999) Transmembrane topography of the 100-kDa a subunit (Vph1p) of the yeast vacuolar proton-translocating ATPase. J Biol Chem 274:14655–14661.

Mirnics K, Norstrom EM, Garbett K, Choi SH, Zhang X, Ebert P, Sisodia SS (2008) Molecular signatures of neurodegeneration in the cortex of PS1/PS2 double knockout mice. Mol Neurodegener 3:14.

Mizushima N, Yoshimori T (2007) How to interpret LC3 immunoblotting. Autophagy 3:542–545.

Mizushima N, Yoshimori T, Levine B (2010) Methods in mammalian autophagy research. Cell 140:313–326.

Muzumdar MD, Tasic B, Miyamichi K, Li L, Luo L (2007) A global double-fluorescent Cre reporter mouse. Genesis 45:593–605.

Neely KM, Green KN, LaFerla FM (2011) Presenilin is necessary for efficient proteolysis through the autophagy-lysosome system in a gamma-secretase-independent manner. J Neurosci 31:2781–2791.

Nishi T, Forgac M (2000) Molecular cloning and expression of three isoforms of the 100-kDa a subunit of the mouse vacuolar proton-translocating ATPase. J Biol Chem 275:6824–6830.

Podlisny MB, Citron M, Amarante P, Sherrington R, Xia W, Zhang J, Diehl T, Levesque G, Fraser P, Haass C, Koo EH, Seubert P, St George-Hyslop P, Teplow DB, Selkoe DJ (1997) Presenilin proteins undergo heterogeneous endoproteolysis between Thr291 and Ala299 and occur as stable N- and C-terminal fragments in normal and Alzheimer brain tissue. Neurobiol Dis 3:325–337.

Prokop S, Shirotani K, Edbauer D, Haass C, Steiner H (2004) Requirement of PEN-2 for stabilization of the presenilin N-/C-terminal fragment heterodimer within the gamma-secretase complex. J Biol Chem 279:23255–23261.

Ratovitski T, Slunt HH, Thinakaran G, Price DL, Sisodia SS, Borchelt DR (1997) Endoproteolytic processing and stabilization of wild-type and mutant presenilin. J Biol Chem 272:24536–24541.

Rubinsztein DC, Cuervo AM, Ravikumar B, Sarkar S, Korolchuk V, Kaushik S, Klionsky DJ (2009) In search of an "autophagomometer." Autophagy 5:585–589.

Ruiz-Canada C, Kelleher DJ, Gilmore R (2009) Cotranslational and post-translational N-glycosylation of polypeptides by distinct mammalian OST isoforms. Cell 136:272–283.

Sardiello M, Palmieri M, di Ronza A, Medina DL, Valenza M, Gennarino VA, Di Malta C, Donaudy F, Embrione V, Polishchuk RS, Banfi S, Parenti G, Cattaneo E, Ballabio A (2009) A gene network regulating lysosomal biogenesis and function. Science 325:473–477.

Saura CA, Choi SY, Beglopoulos V, Malkani S, Zhang D, Shankaranarayana Rao BS, Chattarji S, Kelleher RJ 3rd, III, Kandel ER, Duff K, Kirkwood A, Shen J (2004) Loss of presenilin function causes impairments of memory and synaptic plasticity followed by age-dependent neurodegeneration. Neuron 42:23–36.

Semprini S, Troup TJ, Kotelevtseva N, King K, Davis JR, Mullins LJ, Chapman KE, Dunbar DR, Mullins JJ (2007) Cryptic loxP sites in mammalian genomes: genome-wide distribution and relevance for the efficiency of BAC/PAC recombineering techniques. Nucleic Acids Res 35:1402–1410.

Settembre C, Di Malta C, Polito VA, Garcia Arencibia M, Vetrini F, Erdin S, Erdin SU, Huynh T, Medina D, Colella P, Sardiello M, Rubinsztein DC, Ballabio A (2011) TFEB links autophagy to lysosomal biogenesis. Science 332:1429–1433.

Sherrington R, Rogaev EI, Liang Y, Rogaeva EA, Levesque G, Ikeda M, Chi H, Lin C, Li G, Holman K, Tsuda T, Mar L, Foncin JF, Bruni AC, Montesi MP, Sorbi S, Rainero I, Pinessi L, Nee L, Chumakov I, et al. (1995) Cloning of a gene bearing missense mutations in early-onset familial Alzheimer's disease. Nature 375:754–760.

Shintani T, Klionsky DJ (2004) Autophagy in health and disease: a double-edged sword. Science 306:990–995.

Suzuki K, Kirisako T, Kamada Y, Mizushima N, Noda T, Ohsumi Y (2001) The pre-autophagosomal structure organized by concerted functions of APG genes is essential for autophagosome formation. EMBO J 20:5971–5981.

Takasugi N, Tomita T, Hayashi I, Tsuruoka M, Niimura M, Takahashi Y,

Thinakaran G, Iwatsubo T (2003) The role of presenilin cofactors in the gamma-secretase complex. Nature 422:438–441.

Tanida I, Minematsu-Ikeguchi N, Ueno T, Kominami E (2005) Lysosomal turnover, but not a cellular level, of endogenous LC3 is a marker for autophagy. Autophagy 1:84–91.

Thinakaran G, Borchelt DR, Lee MK, Slunt HH, Spitzer L, Kim G, Ratovitsky T, Davenport F, Nordstedt C, Seeger M, Hardy J, Levey AI, Gandy SE, Jenkins NA, Copeland NG, Price DL, Sisodia SS (1996) Endoproteolysis of presenilin 1 and accumulation of processed derivatives in vivo. Neuron 17:181–190.

Thinakaran G, Harris CL, Ratovitski T, Davenport F, Slunt HH, Price DL, Borchelt DR, Sisodia SS (1997) Evidence that levels of presenilins (PS1 and PS2) are coordinately regulated by competition for limiting cellular factors. J Biol Chem 272:28415–28422.

Thyagarajan B, Guimarães MJ, Groth AC, Calos MP (2000) Mammalian genomes contain active recombinase recognition sites. Gene 244:47–54.

Yen WL, Klionsky DJ (2007) Atg27 is a second transmembrane cycling protein. Autophagy 3:254–256.

Zaidi N, Maurer A, Nieke S, Kalbacher H (2008) Cathepsin D: a cellular roadmap. Biochem Biophys Res Commun 376:5–9.

Zhang Z, Nadeau P, Song W, Donoviel D, Yuan M, Bernstein A, Yankner BA (2000) Presenilins are required for gamma-secretase cleavage of beta-APP and transmembrane cleavage of Notch-1. Nat Cell Biol 2:463–465.